FAR INFRARED SPECTROSCOPY WITH A TUNABLE SOURCE OF RADIATION

F.C. van den Heuvel

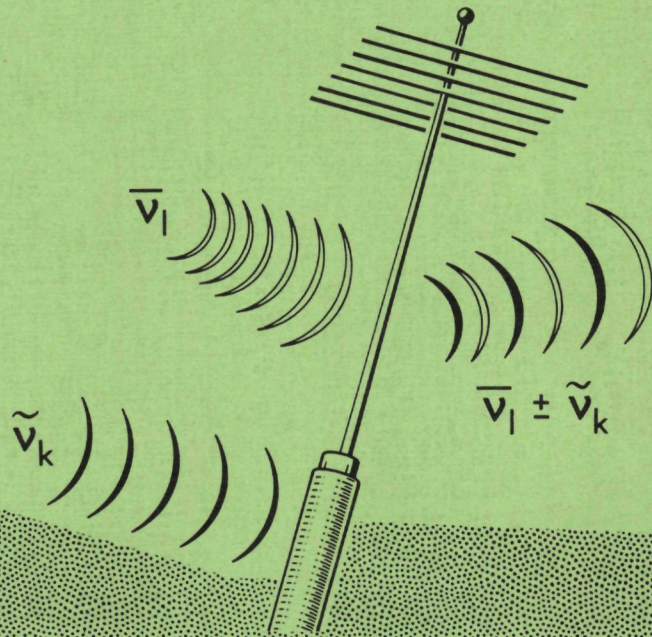$\overline{\nu}_l$

$\tilde{\nu}_k$

$\overline{\nu}_l \pm \tilde{\nu}_k$

FAR INFRARED SPECTROSCOPY WITH
A TUNABLE SOURCE OF RADIATION

FAR INFRARED SPECTROSCOPY WITH
A TUNABLE SOURCE OF RADIATION

PROEFSCHRIFT

TER VERKRIJGING VAN DE GRAAD VAN DOCTOR
IN DE WISKUNDE EN NATUURWETENSCHAPPEN
AAN DE KATHOLIEKE UNIVERSITEIT TE NIJMEGEN,
OP GEZAG VAN DE RECTOR MAGNIFICUS
PROF DR J.H G.I. GIESBERS
VOLGENS BESLUIT VAN HET COLLEGE VAN DEKANEN
IN HET OPENBAAR TE VERDEDIGEN
OP DONDERDAG 21 OKTOBER 1982
DES NAMIDDAGS TE 2 UUR PRECIES

door

FREDERICUS CHRISTIAAN VAN DEN HEUVEL

geboren te Velp

aan mijn moeder
en
ter gedachtenis
aan mijn vader

CONTENTS

CHAPTER 1

INTRODUCTION

1.1 Goal of the project

Primary goal of the investigation described in this thesis has
been the extension of high resolution microwave spectroscopy
into the far-infrared region. This region of the electro-
magnetic spectrum is in prospect of investigations of
molecular species and interactions which are impossible or
very difficult to study in the conventional (long wavelength)
microwave region. Rotational transitions of light molecules
(e.g. hydrides) fall in the far-infrared (FIR) region as do
transitions between highly excited rotational states of
heavier molecules, which are subject to strong centrifugal
distortions or torsional effects (e.g. in CH_3SiH_3). Also
radio-astronomy is pushing farther into the FIR region
because transitions between excited states of a number of
interstellar molecules can be found there. Notable examples
are rotational transitions of CO and inversion transitions of
NH_3 in the excited $v_2=1$ vibrational state. For the present
investigation most important were prospects of spectroscopy
on light free radicals and ions.
       Free radicals play an important role in reaction
chemistry, both terrestrial and interstellar. These molecules
are also interesting for physicists. Radicals are characterized
by an open-shell configuration of the electrons and as a
result, by a non-zero orbital angular momentum and/or electron
spin. Strong interaction between the magnetic fields
associated with these momenta and the nuclear spin(s) results
in large magnetic hyperfine structure in radical spectra.
Analysis of the spectra reveals details of the interactions and
of nuclear and electronic properties. Confrontation of experi-
mental results with theory is an important aid in development
of radical wave functions which in turn can be used to

9

calculate other properties.

Free ions have been subject of numerous investigations, most of them in the visible and ultra-violet region. In contrast with study of radicals, it was not until a few years ago that high resolution ion spectroscopy was initiated in the long wavelength regions. Ion production has been the main problem. In laboratory it is not easy to generate ions at high concentration in a big volume, spectra are generally weak and high sensitivity spectrometers are needed. Only few ions have been investigated in the far-infrared and microwave region till now. Emission of some of them (CO^+, HCO^+, HCS^+ and HNN^+) have been observed from interstellar space. The field of high resolution ion spectroscopy offers interesting prospects for experimental and theoretical research.

It is well known that the absorption coefficient for radiation incident on a gaseous medium containing resonant molecules, is proportional to frequency in case of Doppler-limited spectroscopy and to the square of frequency otherwise. Consequently, a FIR spectrometer is capable of detecting much lower concentrations of (difficult to produce) free radicals or ions than its microwave competitor of comparable sensitivity. Unfortunately this potential advantage was nullified in the past by lack of tunable sources of strong FIR radiation and low sensitivity of detectors in this region. Below we shall discuss some of the problems in more detail and the adopted solutions.

1.2   Sources of far-infrared radiation

Development of high resolution spectroscopy in the FIR region has been seriously hampered by the lack of tunable sources of radiation. The problem of tunability can be evaded by making use of the fact that molecular transitions can be tuned into resonance with a fixed frequency source (laser) by a magnetic field. This method resulted in the development of the technique of laser magnetic resonance. Usually spectroscopy of this type is performed intracavity in optically pumped submillimeter

lasers. Consequently, sensitivity is very high, which makes laser magnetic resonance a powerful technique for detection of small concentrations of free short-lived species. In the FIR the technique has been successfully applied to investigate atoms, diatomic, triatomic and polyatomic radicals (e.g. CH_2OH, RAD 81), metastables and recently also ions (HBr^+, SAY 79). With practicable field strengths, "tunability" is limited to a few GHz around the laser frequency. A drawback of the technique is that application is limited to paramagnetic species only, while interpretation of the usually complex magnetic spectra is often very difficult.

Fourier transform spectroscopy makes use of sources of black-body radiation, that cover the far-infrared range completely. Merit of Fourier spectrometers is the possibility to obtain uninterrupted spectra in a large span of frequencies from a single interferogram (e.g. SAK 78). However, sensitivity and resolution are correlated and limited, primarily by low radiant power per bandwidth. Optimal resolution in the range 10-100 cm^{-1} (0.3-3.0 THz) is of the order of 10^{-4}.

Attempts have been made to generate tunable far-infrared radiation, using infrared sources. Radiation of two tunable infrared lasers has been mixed in a non-linear crystal ($LiNbO_3$) and radiation corresponding to the difference frequency was generated (PAR 78). The method of stimulated Raman scattering in gaseous media has also been applied successfully to generate tunable FIR radiation (MAR 78). In this method Raman active molecules are off-resonantly pumped by a tunable infrared laser to an excited vibrational state. Frequency of scattered Stokes radiation is tunable around the frequency corresponding to an ordinary rotational transition of the molecules in the excited state. Maximal detuning is of the order of 100 GHz. High pump power required for both non-linear mixing and Raman scattering experiments is obtained with pulsed infrared lasers. Yet, both methods are not attractive for spectroscopic application, because bandwidth of generated radiation is too large (of the order of 1 GHz) for high resolution spectroscopy.

The approach from the microwave region is more promising.

At present time, crossed-waveguide mixers are widely used to generate harmonics of the frequency of conventional microwave sources (klystrons, backward wave oscillators, etc.). Although power of generated radiation rapidly decreases with harmonic order, this technique proves very well applicable to high resolution spectroscopy. Microwave spectroscopy has been extended up to 850 GHz (HUY79, PIC 81) using klystrons operating at a frequency in the range 50-150 GHz, and conventional submillimeter detectors. Zuidberg (ZUI 79) estimated that a harmonic generator spectrometer can be operated at frequencies up to 1400 GHz if a heterodyne detector with a laser local oscillator is used. It should be noted, that a heterodyne detector is extremely sensitive (ZUI 78, ZUI 79, FET 78). These devices are also used for radiometric measurements in radio astronomy (CLA 81, ROS 81).

With the advent of electron beam devices operating at frequencies above 200 GHz (backward wave oscillators, carcinotrons), the high frequency limit of microwave spectroscopy has been shifted farther towards the FIR. Nowadays carcinotrons can be operated smoothly in the range 200-500 GHz. They are used on limited scale, because it was not until a few years ago that problems concerning stability of frequency and power control were overcome, while price of these devices is still very high. Attempts are made (WIN 79) to multiply the frequency of carcinotrons with harmonic generators. Carcinotrons operating at frequencies around 1 THz are subjected to continuous improvements by research groups in the Soviet Union. Although it is not easy to operate these ultra high frequency devices and to control frequency, a few interesting high resolution spectroscopic investigations have been carried out with these carcinotrons. For example, the inversion spectrum of ammonia in the excited $v_2=1$ vibrational state has been studied up to 1100 GHz by Belov *et al.* (BEL 80). Unfortunately, the 1 THz carcinotrons are not yet available commercially, but situation might change in the near future.

1.3 Essentials of present spectrometer and results

A few years ago Bičanič (BIC 78, 78a, 81) developed a laser-
sideband generator, a very attractive source of tunable far-
infrared radiation (TFIR). He successfully demonstrated
generation of tunable sidebands of an HCN laser by mixing the
radiation of the laser with that of a 70 GHz klystron in a
mixer equipped with a Schottky barrier diode as non-linear
element. In general, the generated frequency spectrum is
composed of linear combinations $m\nu_1 \pm n\nu_k$ (m,n=1,2,3...) of the
fixed frequency of the laser (ν_1) and tunable frequency of the
klystron (ν_k). Major part of power is transformed into the
fundamental mixing products

$$\nu_{sideband} = \nu_1 \pm \nu_k$$

Beams of TFIR radiation, corresponding to these frequencies,
are radiated by the mixer and can be applied to spectroscopy.
It has been intention of present work, as far as the
instrumental part is concerned, to increase TFIR power and
spectrometer sensitivity, extend the frequency range, simplify
Bičanič's design and lighten operational procedures. Sensitivi-
ty in terms of signal to noise ratio of generated TFIR power
has been improved by two orders of magnitude. The range of
frequencies that could be covered for spectroscopic
investigations, has been expanded to the range shown in Fig.1,
using a hydrogen cyanide and water vapour laser, and ten
available klystrons. It should be noted that only fundamental
mixing products have been used throughout this work. Use of
higher order mixing products goes at the expense of sensitivity.
For example, it was found that power of TFIR is inferior by a
factor of twenty, if the mixer is adjusted for operating at fre-
quencies $\nu_1 \pm 2\nu_k$.
    Sensitivity of the laser-sideband spectrometer is directly
coupled to power level of generated TFIR and more specifically,
to efficiency of the mixer. Since the FIR region is inter-
mediary between the optical and microwave region both optical
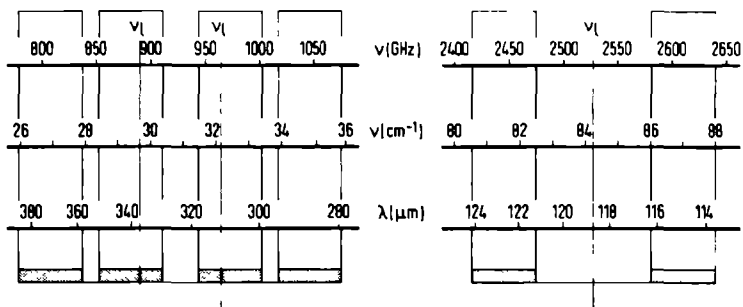
Fig.1 : *Tuning range of spectrometer, with the available lasers (HCN and H_2O) and klystrons. Fundamental mixing ($\nu_l \pm n\nu_k$ with n=1) is assumed.*

and microwave techniques can be applied in designing FIR spectrometers. Bičanič made the approach from the microwave region and used a modified harmonic generator (triple-arm mixer) to produce laser-sidebands. Microwave radiation was transported by fundamental waveguide, far-infrared radiation by oversized waveguides. From experience obtained with Bičanič's mixer in an early stage of this work, and by Zuidberg with a diode mounted in free space (ZUI 77), it was expected that mixer efficiency could be improved employing quasi-optical techniques. Ten times higher output power (1 μW) was obtained with the mixer described in Sect.2.3. At the same time ease of operation of the mixer was enhanced. Its open structure allows good control of miniature-sized diode contacts.

In general the detection system of a spectrometer should be as sensitive as possible. However, excessive complexity of the experimental set-up should be avoided. Although heterodyne Schottky-barrier and Josephson-junction detectors (BLU 79, ULR 78) have a very low noise figure it was decided not to apply this type of detectors for present work. The main reason is that for large and fast scans required in radical and ion spectroscopy the detector should not require frequent time-consuming ad-justments and its frequency response should be flat over the entire range of scans. A composite-type bolometer was used that

14

met these requirements. Sensitivity of present spectrometer is detector-noise limited, but the bolometer allows observation of molecular absorption of radiation equivalent to 10^{-11} W. This quantity corresponds to 10^{-4} times TFIR power incident on the detector. In case of a 1 m long absorption cell this fraction corresponds to a minimum detectable absorption coefficient of 10^{-6} cm^{-1} (RC=0.3 s).

Sensitivity proved sufficient to obtain spectra of radicals in their ground electronic and vibrational state. Spectra have been recorded of nitric oxide (NO), hydroxyl (OD), carbon fluoride (CF), and imine (NH). Fine and hyperfine structure were resolved in most cases and molecular parameters have been determined or determined more accurately. Feasibility of ion spectroscopy in the FIR has been demonstrated. Experimental efforts to find an efficient source for ion production were rewarded with the observation of rotational transitions originating from three ions of astrophysical importance: HCO^+, CO^+, and HN_2^+.

Resolving power of the laser-sideband spectrometer has not been exploited completely. All spectra in this work were recorded with Doppler-limited resolution (3×10^{-6}), while band-width of generated TFIR allows sub-Doppler spectroscopy. Using a laser-sideband spectrometer and molecular beams, Blumberg *et al.* (BLU 81) obtained a resolution of 1.5×10^{-7} at 692 GHz. However, absorption in case of molecular beams is much weaker than in case of cell experiments. Even if a heterodyne detector is used, like Blumberg *et al.* did, decrease of absorption intensity is such, that it is doubtful whether radical and ion spectroscopy in the far-infrared is feasible with higher resolution than obtained in present work.
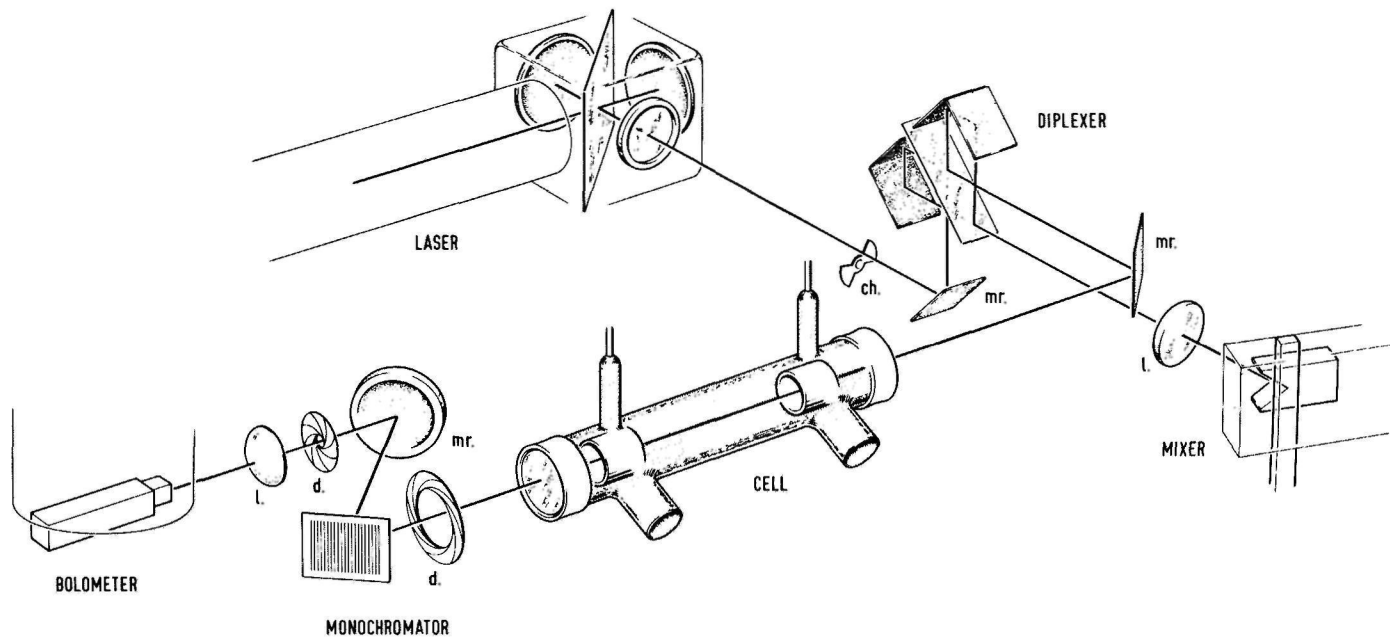
Figure 2 : The far-infrared spectrometer. Ch=chopper, D=diaphragm, L=lens, Mr=mirror.

THE FAR-INFRARED SPECTROMETER

2.1 Outline of the spectrometer

An artists view of the experimental set-up is presented in
Fig.2. The carrier frequency ν_1 of tunable far-infrared
radiation (TFIR) is produced by a submillimeter discharge
laser: a hydrogen cyanide (HCN) laser for the 0.9 THz region
and a water vapour laser for the 2.5 THz region. The
collimated beam of radiation produced by the laser is focussed
onto the active part of a mixer by means of a polyethylene
lens. Microwave radiation of frequency ν_k, produced by a
tunable klystron, is propagated towards the mixer via
ordinary rectangular waveguide. In the mixer diode frequency
mixing takes place, and a beam of TFIR is radiated towards the
polyethylene lens. It coincides with the laser beam incident
on the mixer, but has opposite direction. Spatial separation
of the laser and TFIR beams is accomplished by a folded
Michelson-type interferometer (diplexer), looated between
laser and mixer. The two beams of TFIR, corresponding to sum
and difference frequency $(\nu_1 \pm \nu_k)$, which are not separated
spatially, are transmitted through an absorption cell.

A simple monochromator is used to select either of the
two TFIR beams and to purify it further from fundamental laser
radiation. Finally, the selected beam of TFIR is detected by a
liquid helium cooled bolometer. When frequency is scanned,
resonance of molecules present in the absorption cell directly
appears as a signal from the detector.

All beams of far-infrared radiation in the spectrometer
propagate in open space and are directed by flat mirrors, made
of high quality window-pane coated with gold. Use of wide
collimated beams, with a diameter in the order of a few
centimeters, makes diffraction negligible. The propagation path
from laser to mixer is about 2 m long, including the internal

path of the diplexer; from mixer to monochromator it is about
3 m long, including (again) the diplexer and the 1 m long
absorption cell.

2.2   Lasers and klystrons

2.2.1   The HCN laser (λ=337 and 311 μm)

Most of the spectroscopic studies reported in Chapter 3 have
been performed using an HCN laser as fundamental source of
radiation. For a detailed description of this laser, the
reader is referred to the thesis of Bičanič (BIC 78). The laser
consists of an 8 m long glass tube, terminated by resonator
mirrors. The gain medium is almost as long as the laser, and
contains HCN molecules produced by a DC glow discharge through
a mixture of methane and ammonia. Far-infrared power is
extracted from the resonator by means of a Michelson-type
output coupler (shown in Fig.2), resulting in a linearly
polarized beam of radiation. This polarization is required for
proper operation of the mixer and diplexer (see Sect.2.3 and
2.4). The laser produces a collimated beam with an effective
diameter of about 40 mm. After passing a flat window (made of
TPX), the beam propagates towards diplexer and mixer without
any guidance.
     The laser can operate in different modes and at different
lines, as can be seen from Fig.3. When the Michelson output
coupler is set properly, the laser operates on a single line
and in fundamental TEM_{00q} mode. The two strongest lines were
used for spectroscopy, and correspond to a frequency of 891 and
964 GHz. Highest power of the laser was obtained when the out-
put coupler was equiped with a 40 μm polypropylene foil, and
was in the order of 50 mW at 891 GHz (20 mW at 964 GHz).
     For spectroscopic measurements the frequency ν_1 of the
laser should be known exactly. Although it is more or less fixed,
its precise value can shift within the gain curve of the laser
by as much as a few MHz. In an early stage of the experiment ν_1
was monitored simultaneously with measurements by observation

18
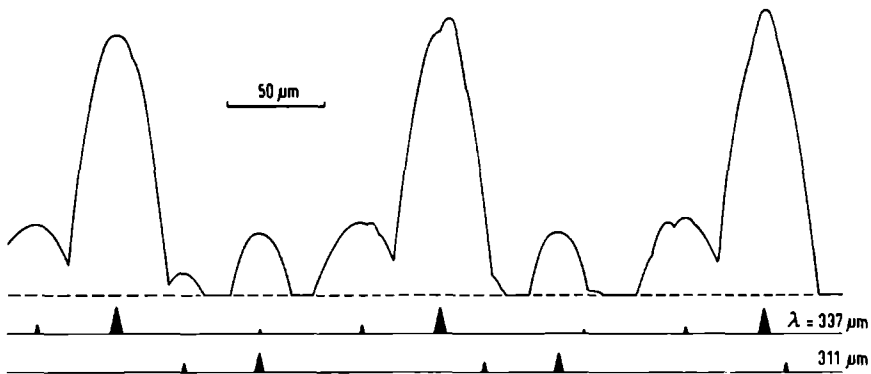
Fig.3 : Output power of the HCN laser versus resonator length. Two strong laser lines are oscillating alternately or simultaneously, the strongest one (λ=337 μm) in three, the other one (λ=311 μm) in two different modes. Small irregularities originate from weak cascade laser lines.

of the beat of the laser with a harmonic frequency of a klystron, generated in a secondary mixer (HEU 80). In principle, the laser could have been locked in a similar way to a low-frequency standard, but it was chosen not to do so in favour of reduced complexity of the set-up. The short term stability of the free running laser was determined by Zuidberg (ZUI 77). Under stable discharge conditions he found a value of 10 kHz for the width of oscillation, which is far beyond requirements set by spectroscopy in a cell where absorption lines are Doppler broadened to a few MHz. Slow drift of frequency caused by thermal expansion of the resonator could be neglected during measurement of an absorption line. Before each spectroscopic measurement the laser manually set at the top of the gain curve. It was found that with this setting the laser frequency was within 1 MHz equal to:

ν_1 = 890 760.3 MHz for the 337 μm line
ν_1 = 964 312.7 MHz for the 311 μm line

19

The spectral range that could be covered using these two
carrier frequencies of the HCN laser and the available
klystrons, is illustrated in Fig.1.

2.2.2   The H_2O laser (λ=118.6 μm)

The mechanical construction of the water vapour laser used in
the experiment described in Sect.3.5, is almost identical to
that of a 4 m HCN laser described by Bičanić (BIC 78). A 4 m
long glass tube contains the gain medium, and is cooled by tap
water flowing through a coaxial jacket. The semi-confocal
resonator consists of a concave mirror (8 m radius of
curvature) at the cathode end and a flat mirror at the anode
end. The latter mirror forms a part of a Michelson-type output
coupler. All mirrors are made of glass and gold coated. In
order to obtain a stable and reliable discharge through the
gain medium, the laser is equiped with a copy of the cathode
used for the 8 m HCN laser (Sect.2.2.1). This hollow cathode is
the outlet of the vacuum system, and since it is twice as wide
as the cathode originally designed for the 4 m HCN laser, it
allows a higher flow of the laser medium. This fact proved to be
very important as will be explained later. The anode consists of
a solid ring of stainless steel, placed in a wide part of the
plasma tube near the output coupler. The internal diameter of
the ring was chosen slightly larger than the bore of the plasma
tube, in order to avoid interception of part of the laser beam.
The mirrors of the output coupler could be translated and tilted
for accurate angular alignment by means of mounts designed by
E.van Leeuwen. The mirror near the high voltage electrode
(cathode) could only be oriented in a more primitive way by
compression of the vacuum seal ("O"-ring) between mirror and
framework of the laser. This mirror needed extra care when the
laser was assembled and optical alignment (with diaphragms and
a He-Ne laser) was done under vacuum conditions. The Michelson
output coupler (beam splitter) could be replaced by a small
mirror at an angle of 45° with respect to the laser axis. This
mirror could be inserted into the resonator at any desired

distance from the axis, so as to extract laser power with resonator losses as low as possible. This method of output coupling proved to be very convenient for adjusting the laser.

In literature extensive descriptions of the operational characteristics of a CW water vapour laser can be found (e.g. BRA 72, WOS 75), but most quantitative data are only relevant to the specific laser described. There is strong correlation between various conditions of the gain medium (chemical composition, total pressure, discharge current, flow rate) and the actual geometry of the plasma tube (volume, length, position of inlet and outlet). Although information from literature was useful as a guide-line in early stages, optimal conditions were found by trial and error procedure. Laser oscillation at $\lambda=28$ μm and 79 or 118 μm was easily obtainable if power was coupled out with the auxiliary mirror, but difficulties arose when the mirror was replaced by a beam splitter. Laser action at 118.6 μm could only be obtained using a thin (about 7 μm) foil of polyethylene cut from a sandwich bag (!), probably because of high purity of the material.

It was noticed that laser power became more and more sensitive to small changes of total and partial pressure when the laser was pushed to high power operation. Highest possible current was desirable for high output power,which in turn dictated high gas flow. In an effort to obtain higher power at $\lambda=118.6$ μm two plasma tubes have been compared, one of 75 mm and another of 50 mm bore. About three times higher power has been obtained with the 50 mm tube, probably because of higher current density. The ultimate power level, set by the current limit of the laser power supply, was in the range of 5-10 mW and obtained from a 0.9 A discharge through a mixture of water vapour and hydrogen at a total pressure of 100-250 Pa. A high and constant flow of gas was maintained by a 30 m^3/h rotary pump. The optimal conditions for operation were easily reproducible, resulting in a very reliable laser, with a higher long term stability than the long HCN laser.

For spectroscopic measurements the following frequency (FRE 67) was accepted for the center of the gain curve:

$$\nu_1 = 2\ 527\ 952.8(3)\ MHz$$

2.2.3 Klystrons and microwave equipment

Ten reflection-type millimeter wave klystrons were available
for experiments, almost completely covering the frequency range
from 53 to 112 GHz. Each of them delivered a power of 40-400 mW
over a tuning range of 3-10 GHz. All klystrons could be locked
to a reference oscillator with a double-loop phase-lock system,
described elsewhere (DIJ 71). Two K-band klystrons, operating
at 18-26 GHz, were used as intermediate oscillators to lock the
high frequency klystrons to the reference oscillator (Rohde &
Schwarz frequency synthesizer, XUC). During experiments
different methods have been applied to scan the frequency of
the klystrons. The full phase-lock system, with scanning
reference oscillator, was used for small scans only. For large
scans (of the order of 1 GHz) the high frequency klystrons were
used in free-running condition. Their frequency was compared
with the fixed reference oscillator, while scanning the klystrons
either mechanically or electrically. Accurate mechanical tuning
was feasible for only few klystrons, and usually smooth scans
were made by electrical tuning. For the latter method the power
supply of the klystrons was modified in such a way that a slow
ramp could be superimposed on the reflector voltage. Electrical
tuning range was 50-200 MHz.

During spectroscopic investigations it was experienced
that klystron sources are not very well suited for present
application in the far-infrared region. One striking example is
the problem associated with frequency modulation, which has been
applied many times. The width of an absorption line of molecules
detected in a cell is at least ten times larger at 1000 GHz than
at the fundamental frequency of the klystron in use. The
modulation depth required for far-infrared studies is then in
the order of a few MHz, and is not negligible with respect to
the width of the electrical tuning range of the klystron. This
causes also amplitude modulation of the generated TFIR power,
resulting in spurious signals (curved base-line). An additional

problem with strong frequency modulation is, how to force the
klystron to oscillate with modulated frequency while locked to
a reference oscillator. In phase-lock systems used in micro-
wave spectroscopy this is accomplished by modulation of the
reference oscillator, but at high modulation depths a
conventional phase-lock system is not suitable any more. The
only way out was to operate the klystrons free-running with
the frequency modulation voltage directly applied to the
reflector via its power supply.

From the description given above it is clear that the
power of generated TFIR and the ease of tunability was directly
related to the individual operating characteristics of each
klystron.

2.3 Open mixer

2.3.1 Mechanical construction

An elucidating view of the mixer is shown in Fig.4. The active
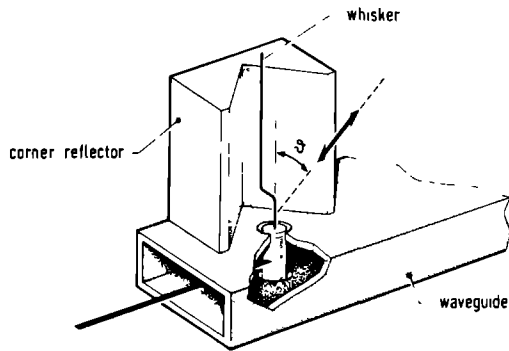
Fig.4 : Cross-sectional view of the open mixer.

element of the mixer is a diode chip, mounted on top of a
golden stud with a diameter of 0.7 mm. The stud is electrically
isolated from a mounting block and can be raised to any

23

potential via a BNC connector attached to its suspension. Micro-
wave radiation propagates towards the diode via a rectangular
waveguide fitted into the block, parallel and close to the
surface (cf. Fig.2). The stud, centered in the waveguide,
functions as antenna for microwave radiation. Impedance
matching is accomplished by a plunger which terminates the
waveguide. Far-infrared radiation is transmitted towards and
from the chip via a thin whisker antenna contacting a diode on
top of the chip. The whisker is attached to a pin, and can be
positioned accurately with respect to the chip by means of
differential screw mechanisms. A corner reflector is placed
behind the whisker, and the separation between them is
adjustable by means of a translational stage fitted into the
mounting block. The mixer is supported by three (x,y,z-)
translational stages for accurate positioning of the whisker
into the focal point of a polyethylene lens (shown in Fig.2),
whereas the angle θ between laser beam and whisker can be varied
continuously by rotation of the complete mixer around an axis
parallel to the waveguide.

2.3.2 Microwave part

This part of the mixer does not differ from the conventional
design of a harmonic generator (DIJ 71). The stud of the diode
chip functions as receiver of microwave radiation and is
positioned in the center of the waveguide. During experiments
both WR-10 (75-110 GHz) and WR-12 (60-90 GHz) waveguides have
been used, each of them fitted to a separate mixer block. Micro-
wave radiation was coupled most efficiently to the diode when
WR-12 waveguide was used, probably because of better impedance
matching of the stud to the larger waveguide. In fact, the
complete frequency range 53-112 GHz could be covered with just
the WR-12 waveguide, when the stud was carefully positioned.
Best operation of the mixer was obtained with a relatively large
hole (1 mm) in the top wall of the waveguide and rather low
position of the stud, so that the whisker slightly penetrated
into the interior of the waveguide. The waveguide wall was made

as thin as possible ($\leq$ 0.1 mm) in order to reduce deterioration of the quality of the whisker as antenna for far-infrared radiation. The optimal configuration indicates partial coupling of microwave power to the diode via the whisker.

2.3.3 The far-infrared part

Fundamental power from the laser is injected to the diode contact via the whisker, whereas the same whisker emits TFIR produced by the diode. The antenna characteristics of a whisker as part of a submillimeter receiver have been studied extensively by Kräutle *et al.* (KRA 77,78) and the construction of the far-infrared part of the mixer is based on their quasi-optical design. They showed theoretically and verified experimentally at λ=337 µm, that the receptance of an antenna in the far-infrared region is most efficient when its effective length ℓ is in the order of a few wavelengths, and when radiation is focused as sharply as possible onto the antenna. At the same time the incident beam should geometrically match the pattern of reception that characterizes such an antenna. According to reciprocity theorem the antenna pattern for reception is identical with that for emission, and implies that TFIR is radiated with an analogous distribution in space.

A free antenna radiates with cylindrical symmetry, and electric field emitted in θ-direction is given by the formula (JAS 61) :

$$E(\theta) \propto \frac{\ell}{\lambda} \sin \theta \; \frac{\sin \pi(1-\cos \theta)\ell/\lambda}{\pi(1-\cos \theta)\ell/\lambda} \tag{2-1}$$

where 2 θ is the top angle of a cone of which the axis coincides with the antenna wire. The radiation is polarized with the $\vec{E}$-vector in the plane suspended by wire and wavevector $\vec{k}$. In Fig.5 $|E|^2$ is plotted as a function of θ for ℓ/λ=7. When the ratio ℓ/λ decreases, the number of conical lobes diminishes and a pronounced main lobe appears at a certain (low) value of the angle θ. The effective cross-section of the whisker for the incident laser beam should be as large as possible. Therefore
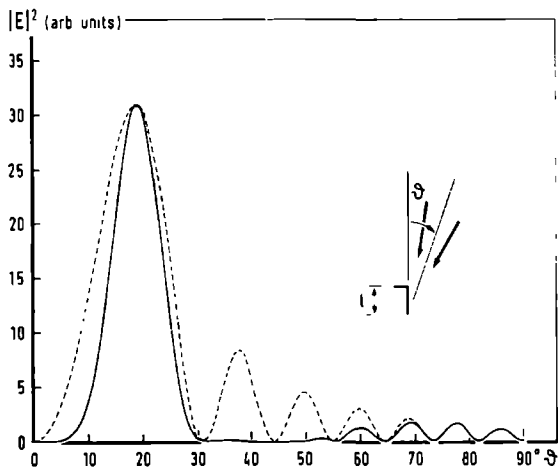
Fig.5 : *Pattern of an antenna in free space (dashed curve) and backed up by a corner reflector (solid curve).* $|E|^2$ *is plotted as a function of the angle of incidence* θ *for* $l/\lambda=7$, $d/\lambda=1.5$, $\varphi=0$.

the ratio l/λ should be chosen such that the focused beam completely falls within the solid angle suspended by the main lobe of the antenna pattern. At the same time, TFIR emitted by the whisker should be transformed into a smooth directional beam as efficiently as possible. The latter requirement is not compatible with the cylindrical symmetry of the antenna pattern. Kräutle *et al.* (KRA 77,78) extensively investigated the effect of reflectors behind a receiver antenna, and found very satisfactory results with corner reflectors, both with respect to directivity and to efficiency. The antenna pattern corresponding to a combination of whisker and corner reflector can be calculated via superposition of the driving antenna and an array of its images. In case of a 90° corner reflector, there are three images, and field distribution can be expressed approximately by the formula (FET 78) :

$$E(\theta,\varphi) = E(\theta) \; [\cos(2\pi \, \sin\theta \, \cos\varphi d/\lambda) - \cos(2\pi \, \sin\theta \, \sin\varphi d/\lambda)] \tag{2-2}$$

26

where φ is the azimuth angle with respect to the plane of
symmetry of the corner reflector, and d is the speration between
whisker and vertex of the reflecting planes (see Fig.6a). The
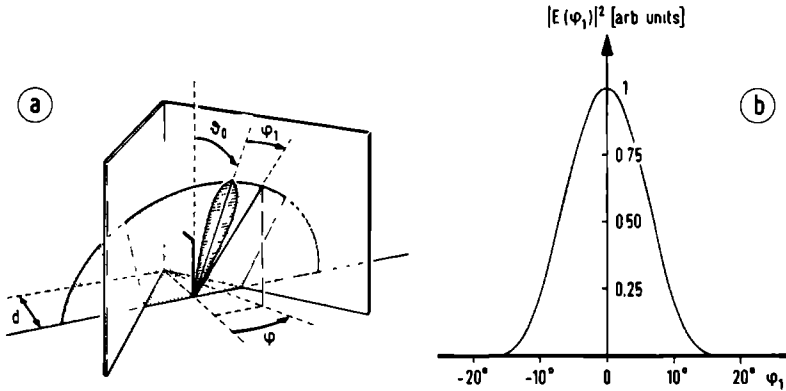
Fig.6 : *Cross section of the main lobe of the antenna pattern presented by*
the solid curve in Fig.5.
(a) Cross-sectional plane defining the azimuthal angle φ_1
(b) $|E|^2$ as a function of φ_1.

effect of the corner reflector is a modulation of the free
antenna pattern by a φ (and θ) dependent part. By proper choice
of d/λ the main (conical) lobe of the free antenna is squeezed
to a highly directional lobe of (almost) circular cross section,
whereas side-lobes are suppressed at the same time. This is
illustrated in Fig.5 and Fig.6b for d/λ=1.5 and ℓ/λ=7.0. The
corner reflector thus favours the collection efficiency for
generated TFIR. However, Eq.(2-2) does not take into account
the match of the whisker/reflector system to the size of the
focal point (spot size) of the focusing optics (a polyethylene
lens) in front of the mixer. Eq.(2-2) is only valid and the
efficiency of the mixer is only enhanced by the corner reflector,
if both the whisker and its mirror images are positioned within
the focal spot. In that case the effective cross section of the
whisker for incident laser radiation is enhanced by its three

27

images, and TFIR generated by the images is efficiently
collected by the lens.

For the plano-convex lens in use, the spot size is
determined both by diffraction and spherical aberration. It was
calculated that minimal spot size could be obtained with a lens
of 100 mm focal length, for the effective diameter of the laser
beam of 40 mm at 0.9 THz, and 25 mm at 2.5 THz. The calculated
spot size was 2.0 mm at 0.9 THz, and 0.6 mm at 2.5 THz. A
compromise between the requirements stated above was found by
choosing the parameter l/λ between 6 and 8, and $d/\lambda \approx 1.5$. Then
the antenna pattern is composed of mainly one lobe directed at
an angle $\theta \approx 20^{\circ}$ (see Fig.5). The whisker was set at this angle
with respect to the incident laser beam by rotation of the
complete mixer. The continuously adjustable parameter d was set
at its proper value, corresponding to (almost) circular cross-
section of the main lobe (cf. Fig.5 and 6). The lobe suspended
a solid angle large enough to contain the full cone of incident
focused laser radiation.

It should be noted that the difference between the antenna
patterns corresponding to incident radiation of frequency ν_1
and emitted TFIR of frequency $\nu_1 \pm \nu_k$ is small, since $\nu_k << \nu_1$.
When the laser was set for maximal collection efficiency for
laser radiation, the efficiency of emission of TFIR was maximum
as well. Also a small directional difference between in- and out-
coming beam of radiation was not correlated with loss of TFIR,
because the active part of the mixer was in the focal point of
the lens that collimated the beam of TFIR.

2.3.4   Diode chips and whiskers

Diode chips from different manufacturers have been tried. Al-
though all of them proved to be suitable for generation of TFIR,
the ultimate power level obtainable with various chips differed
considerably. Schottky barrier (SB) type diodes on a Si substrate,
supplied by dr. C.de Kort from the Solid State Group of professor
P.Wyder, SB diodes on a GaAs substrate, obtained from Alpha
Industries, and GaAs point-contact diodes, they all turned out

to be of inferior quality when compared to chips supplied by dr. H.Fetterman from Lincoln Laboratories, M.I.T. (USA). These chips, especially designed for microwave detectors, consist of arrays of SB diodes on top of a GaAs substrate. A detailed description can be found elsewhere (CLI 71). All spectroscopic investigations presented in Chap.3 have been carried out using two chips of this type.

The whiskers used in experiments were made of 50 μm wire attached to a stud. The end of a whisker was electrolytically etched to a conical point with a half-top angle of about 12°. The tip was slightly blunted to a diameter of the order of few microns at the end of the etching process, in order to reduce its deformation when contacted with one of the diodes of the chip. In favour of mechanical stability the total length of the whisker was kept below approximately 8 mm, whereas the effective antenna length (ℓ) was fixed by making a sharp double bend at a distance ℓ from the whisker tip (see Fig.4 and 5). Both tungsten and gold-copper have been used as whisker materials. Tungsten whiskers were coated with silver or gold to improve electrical conductivity of the material. At 0.9 THz tungsten whiskers have been used most frequently, because of higher mechanical strength of the tip, while the electrical performance was not inferior to that of gold-copper whiskers. At 2.5 THz only gold-copper whiskers were used.

Highest efficiency of the mixer was obtained with the smallest diodes available on the chips, probably because of lower junction capacitance (WRI 78). The diameter of the available diodes varied from 1.5 to 7 μm. Before a diode contact was established the whisker tip was manipulated towards a small diode, while observing the open mixer with a stereo microscope of high brightness. Use of small diodes offered the secondary advantage of high mechanical stability of the contact. Usually one diode contact could be used over a period of one week up to two months, without serious deterioration of the diode performance.

It was found that the quality of a diode as generator of TFIR can not be seen from its I-V characteristic; the procedure to check the quality will be discussed in Sect.2.5.3.

2.4 Diplexer

From Sect.2.3.3 it is obvious that some device is needed to
separate the fundamental laser beam incident on the mixer from
the coinciding beam of TFIR that is radiated by the mixer. Such
a directional coupler should spatially separate the two beams
without losses. An instrument that meets these requirements is
shown in Fig.7, and was originally used by Erickson (ERI 77) to
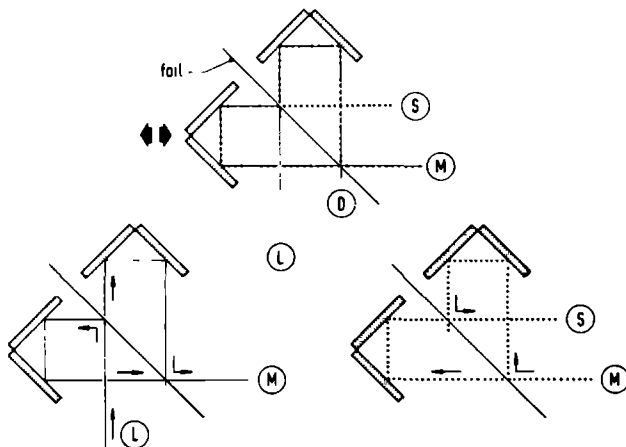
Fig.7 : *Composite diagram of the diplexer.*
Laser beam is guided from port L towards mixer port M, radiated
beam of TFIR from port M towards spectrometer port S (dummy port
D not in use).

combine two beams of far-infrared radiation from a source and
local oscillator in a detection system. It consists of a folded
Michelson-type interferometer, composed of a 45° beam splitter
and two 90° corner reflectors. The laser beam enters the diplexer
via port L and is split into two partial beams by the beam
splitter. Each beam traverses a separate arm of the diplexer and,
after recombination, one beam is directed at the mixer placed
behind port M and a second one leaves the diplexer via the dummy
port D. In an analogous way the beam of TFIR that enters the

diplexer via port M gets distributed over port L and the spectro-
meter port S. Distribution of power to the various ports of the
diplexer depends on the difference in path length of the two
interferometer arms; ideal situation corresponds to 100%
transmission of laser radiation from port L to M, and 100%
transmission of TFIR from M to S. Both incoming beams are then
spatially separated without loss of laser power via port D and
TFIR power via port L.

In case of a lossless beam splitter with power coefficient
of reflection r the coefficients of transmission between port
L and M, or M and S are given by

$$T(L,M) = T(M,L) = 2r \ (1-r) \ (1+\cos k_1 x) \tag{2-3}$$

$$T(M,S) = T(S,M) = (1-2r+2r^2) - 2r \ (1-r) \ \cos k_s x \tag{2-4}$$

where x is the difference in path length between the diplexer
arms, and the wavenumber k_1 and k_s corresponds to the frequency
ν_1 and $\nu_1 \pm \nu_k$ of laser and TFIR, respectively. The requirement
of lossless transmission of laser and TFIR power are met if
r=0.5. There is also the condition that both T(L,M) and T(M,S)
should equal to unity at the same setting of the parameter x.
In principle this only happens when x is a multiple of both
λ_1 and λ_s, but since $\lambda_1 \approx \lambda_s$ there is a more useful criterion,
which will be given below.

A remarkable feature of the diplexer is that it does not
only separate two beams of radiation of roughly the same
frequency, but it also serves as an isolator for one of them.
From Fig.7 is is seen that laser radiation can be transmitted
from port L to port S only indirectly, by reflection on optical
components and the mixer, both placed at port M. However, from
Eq.(2-3) and (2-4) it can be seen that T(M,S)=0 if T(L,M)=1, k_s
in Eq.(2-4) is replaced by k_1 and r=0.5 is assumed. So, in
principle, no fundamental radiation from the laser can be
expected at port S. An additional and sometimes very convenient
property of the diplexer is that it can be used as control unit
of mixer performance. In that case, the power of TFIR at port S
is recorded, while scanning the path length difference x.

31
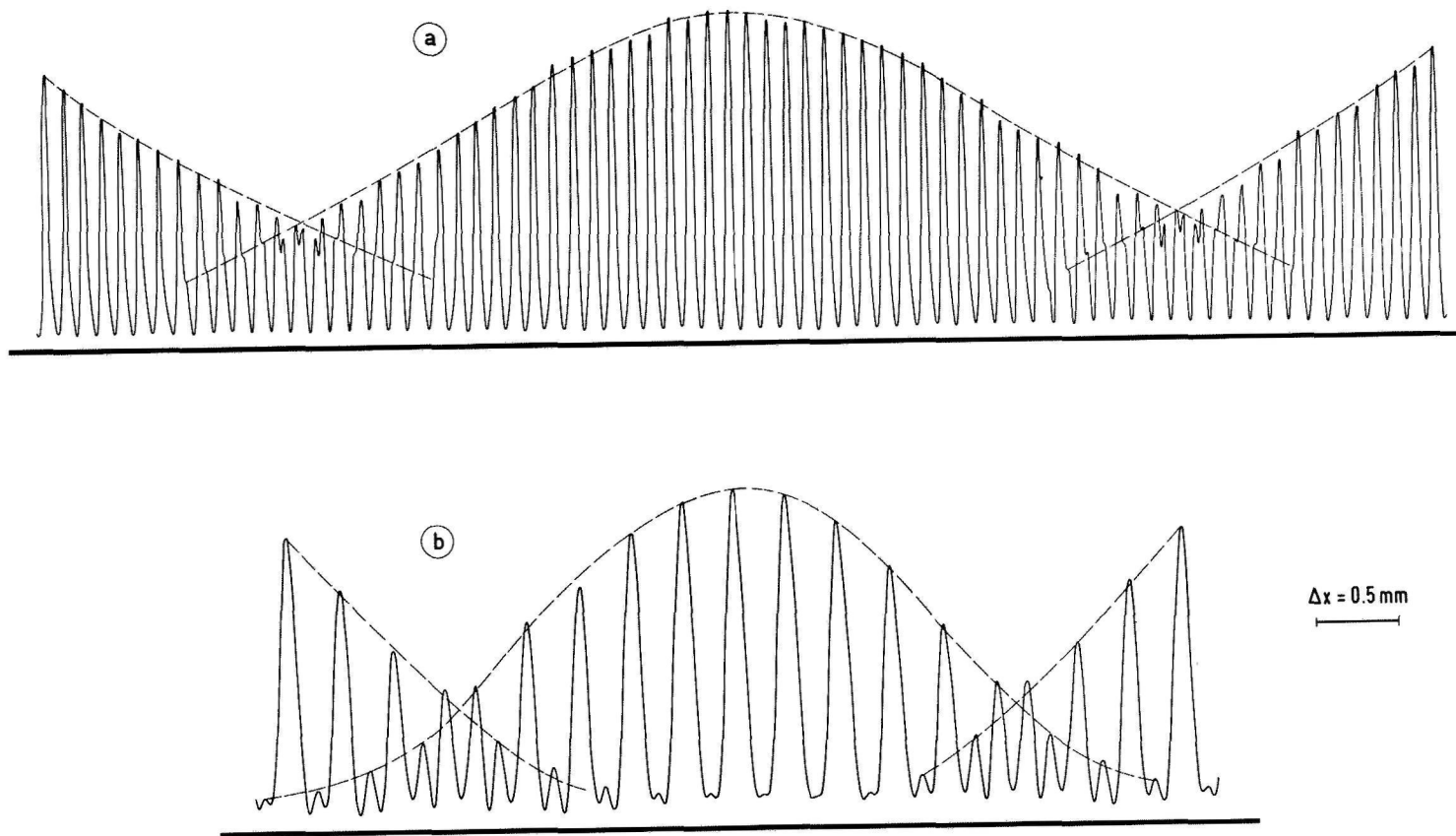
Figure 8 : *Interferogram of the diplexer. Power of TFIR is recorded at port S, with*

(a) $\lambda_l = 337$ μm and $\lambda_k = 3.33$ mm (90 GHz)

(b) $\lambda_l = 118$ μm and $\lambda_k = 5.45$ mm (55 GHz)

$\Delta x = 0.5$ mm

Radiation detected at port S can immediately be identified as
TFIR when the interferogram possesses the characteristic
structure shown in Fig.8. This structure is produced by a
combination of transmission properties of the diplexer and of
mixing process in the diode.

It was found that the power level of generated TFIR is
proportional to the laser power incident on the mixer.
Consequently, the power level detected at port S is proportional
to $T(L,M)$ $T(M,S)$, which for $r=0.5$ is given by:

$$T(L,M)\ T(M,S) = (1/4)\ \{\sin[\pi(\nu_s+\nu_1)x/c] + \sin[\pi(\nu_s-\nu_1)x/c]\}^2$$

(2-5)

When the variable x is scanned, the first term is responsible
for fast oscillations of power and the second for a slowly
oscillating envelope, because $|\nu_s-\nu_1|=\nu_k<<\nu_1$. The period of
oscillation of the terms equals λ_1 (approx.) and λ_k,
respectively, where λ_k is the wavelength in air of the klystron.
This theoretical structure has been verified both at 0.9 THz
and 2.5 THz, and the results are shown in Fig.8. From Fig.8 it
can be seen that it is always possible to find a setting of the
parameter x for which $T(L,M)$ $T(M,S) \approx 1$: the setting should be
chosen within a range λ_1 around a value x' for which the second
(slow) term in Eq.(2-5) equals ± 1. The value x' is given by

$$x' = (2m+1)\ \lambda_k/2 \qquad\qquad m=0,1,2,\ \ldots \qquad\qquad (2\text{-}6)$$

The diplexer used in experiments consisted of a beam
splitter made of thin mylar foil stretched in an aluminium
frame, and mirrors made of glass coated with gold. The components
were attached to a 30×30 cm aluminium plate. All mirrors could
be aligned with precision screws, and one corner reflector could
be translated for adjustment of the variable x. The dimensions
of the apparatus allowed for transmission of beams with
diameters up to 60 mm. Only one material (mylar) was used for
beam splitters, because of its high refractive index and low
absorption loss. It can be shown that at 45° angle of incidence

a multiple-pass reflection coefficient r of 0.5 can only be
obtained if radiation is polarized perpendicularly to the plane
of incidence, and if the single-pass (power-) coefficient of
reflection of the beam splitter material is 17.2% at least.
This demands a refractive index of at least 1.85. Mylar, with
an index of 1.7, very closely meets this requirement. The
thickness of two selected foils was 50 μm for use around 0.9
THz, and 25 μm for 2.5 THz, corresponding to a (calculated)
coefficient of reflection r=0.43 in both cases. From Eq.(2-3)
and (2-4) it follows that in that case the maximal transmission
for TFIR is still 100% and for laser radiation 98% (!),assuming
no material losses. The latter figure was verified and confirmed
experimentally at 0.9 THz, whereas a deviation (about 10%) was
found at 2.5 THz caused by absorption of power by the foil.

   In practice the diplexer turned out to be a very reliable
device. The symmetry of the mirror configuration not only
guarantees high stability with respect to thermal expansion, but
also proper match of wavefronts when two partial beams of
radiation recombine at the beam splitter.

2.5   Detection of tunable far-infrared radiation

2.5.1   Bolometer detector

A helium cooled bolometer has been used for detection of TFIR,
because of its high responsivity, low noise level, flat response
over a large frequency range and ease of operation. Excellent
performance has been obtained using a composite-type bolometer,
commercially available from Infrared Laboratories. It consists
of a germanium element attached to an absorbing substrate and
mounted in an integrating sphere. The internal optical system
of the bolometer is shown in Fig.9. At 1.5°K the electrical
resistance of the element is very sensitive to temperature
changes, and power fluctuations of incident radiation are
directly transformed into corresponding fluctuations of the
voltage across the element when biased by a DC current. In
general there are many degrees of freedom in the design of a
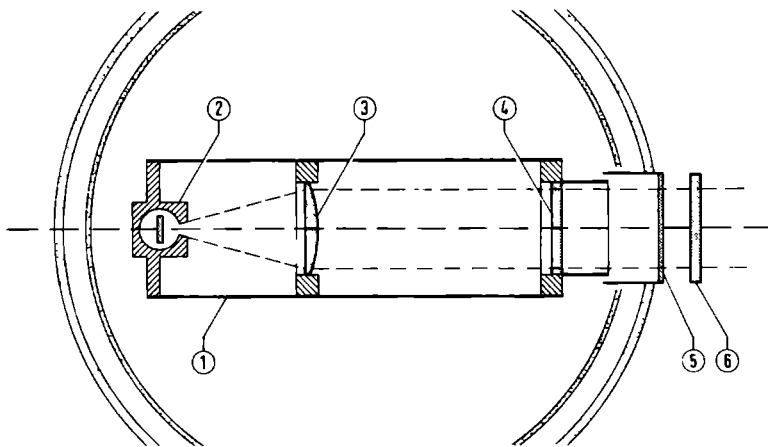
Fig.9 : Lay-out of the bolometer.

    (1) Baffle box attached to cold plate (1.5°K)

    (2) Bolometer element in an integrating sphere

    (3) Crystal quartz lens

    (4) SrF_2 cut-off filter

    (5) Black polyethylene filter attached to radiation shield (LN_2 temperature)

    (6) White polyethylene window (at room temperature).

bolometer system, and within certain limits a bolometer can be matched to the specific requirements stipulated by experimental application. For present experiments special attention has been payed to minimization of the noise level of the bolometer. All possible sources of noise have to be considered (ZWE 68), since without precautions their relative contributions to the overall noise level are of the same order of magnitude. Johnson noise is an inevitable electrical source of noise caused by statistical fluctuations in the motion of charge carriers. It is present in the bolometer element itself, the series resistance of the bias circuit, and the input resistance of the preamplifier. Statistical fluctuations of temperature contribute to electrical noise too (the element electrically responds to temperature changes).

These fluctuations originate in the weak thermal contact of the element with a heat sink at 1.5° K, and in the fluctuations in the number of background photons absorbed by the bolometer. Black body radiation emitted by environment of the detector at 300° K is the main source of background photons. It should be noted that an ideal black body at 300° K radiates about 50 mW/ cm^2 within a hemisphere.

The overall noise level was minimized by a proper choice of various parameters and use of an adequate optical filter section (at 1.5° K) in front of the element. At the same time the manufacturers used their experience to find a compromise between conflicting requirements, such as low noise level combined with high responsivity and reasonable high response speed. The internal optical system of the bolometer, shown in Fig.9, acts as a $\lambda=60$ µm cut-off filter and reduces incident background power to approximately 1 µW.

The various sources of noise contribute to the noise level of the bolometer system in the following way. When referred to the square of the noise voltage V_{rms} at the input of the pre-amplifier, about 75% is caused by the element itself (45% electrically, 30% thermally). The complementary 25% originates from the preamplifier, background photons and load resistor of the bias circuit, in sequence of importance. It was found that the measured value of the noise voltage $V_{rms}=20$ nV/$Hz^{\frac{1}{2}}$ exceeded its calculated value by only a factor of two. It is customary to specify the noise equivalent power (NEP) of a bolometer as V_{rms} divided by the DC responsivity of the element, assuming 100% efficiency of the overall system for transformation of incident radiative power into thermal energy of the element. Given a responsivity of 70 mV/µW this so-called electrical NEP equals 3×10^{-13} W/$Hz^{\frac{1}{2}}$. However, when the specified efficiency of the element (65%) and the transmissivity of the optical system (33%) are taken into account, the optical NEP equals 1.3×10^{-12} W/$Hz^{\frac{1}{2}}$. Finally, the bolometer can only be used in AC operation, and responsivity decreases with increasing modulation frequency because of limited response speed. The real NEP under normal operating conditions is 8×10^{-12} W/$Hz^{\frac{1}{2}}$.

2.5.2 Monochromator

Before the beam of TFIR was admitted to the bolometer, it was necessary to filter it from fundamental laser radiation. In Sect.2.4 it was stated that, in principle, the diplexer prevents transmission of laser power from laser or mixer port towards its exit port. However, the slightest deviation from ideal performance would obscure the observation of TFIR, because there is a difference of four orders of magnitude between power level of the laser and of generated TFIR. For this reason the beam of far-infrared radiation that propagated from diplexer via absorption cell towards detector (see Fig.2), was inter- cepted by a modified version of Bićanić's monochromator (BIC 78). The collimated beam passed a diaphragm (diameter up to 50 mm), and was refracted by a reflection grating (echellette, blaze angle 31°, 3 grooves/mm). Either one of two beams of TFIR corresponding to a frequency $v_1 - v_k$ or $v_1 + v_k$ could be selected and separated from fundamental radiation of frequency v_1 by rotation of the grating. A spherical mirror collected the selected beam and focused it onto a variable diaphragm with a diameter of a few millimeters. Finally, a small polyethylene lens recollimated the beam to a diameter adapted to the internal optical system of the bolometer. It was found that at the input of the monochromator the power difference between a beam of TFIR and fundamental radiation was roughly two orders of magnitude; good filtering of TFIR was only obtainable with the monochromator when supported by the isolating property of the diplexer (cf. Sect.2.4).

Resolution of the grating was sufficient, but rather poor in present application. Usually resolving power is defined as the ratio $v/\Delta v$, where Δv is the smallest resolvable frequency difference when two monochromatic beams are incident on the grating, and is just given as the product of diffraction order k and number of intercepted grooves on the grating surface. In the present situation the grating was used in first and third order (k=1,3) at 0.9 and 2.5 THz, respectively, corresponding to $\Delta v \approx 5$ GHz at both frequencies. However, the calculation of

this figure is based on the assumption of equal intensity of the incident beams, which was clearly not the case in the present experiments. When this fact is taken into account, it can be estimated that two beams of radiation with a frequency difference of 50 GHz can only be distinguished if their intensity difference at the monochromator entrance does not exceed about three orders of magnitude.

Another characteristic parameter of the grating is its angular dispersion $\delta\nu/\delta\gamma$, where $\delta\gamma$ is a small angular displacement of the grating corresponding to a frequency shift $\delta\nu$. For the grating in use the dispersion was 27 GHz/degree at 0.9 THz, and 65 GHz/degree at 2.5 THz. These rather large values indicate the practical limitation of the grating.

2.5.3 Operational procedure

When the spectrometer was adjusted for spectroscopic measurements, the following procedure was followed to ascertain good operation of the mixer. At first the mixer was used as video detector of laser radiation, i.e. the rectified high frequency current in the diode junction induced by the laser was measured. Phase sensitive detection proved to be very convenient and the laser beam was modulated with a frequency of 20 Hz by a mechanical chopper (see Fig.2). At this stage no microwave power was admitted to the mixer and for maximum video signal the DC bias voltage of the diode was adjusted close to the sharp bend of its I-V characteristics. At the same time the path difference of the diplexer was set at its proper value, and the orientation and position of the mixer was adjusted for maximal video signal. This procedure assured good match of laser radiation to the mixer antenna, and efficient emission of TFIR as well.

At this stage the quality of the diode contact was considered. Experience showed that the strength of the video signal was the most reliable measure of anticipated TFIR power. A diode contact was rejected and a new one established in case the obtained video signal deviated far from an ultimate level

known from earlier experience. Microwave power was then admitted to the diode and the generated beam of TFIR was detected by the bolometer. Again phase sensitive detection was applied, but with a modulation scheme that prevented simultaneous modulation of TFIR and of laser power reaching the bolometer. A square wave voltage was superimposed on either the bias supplied to the mixer diode or on the reflector voltage of the klystron. In both cases the amplitude of the wave was chosen such, that power of TFIR was switched on/off periodically. It was not possible to obtain full suppression of modulation of laser power with either scheme, and use of the monochromator was essential. After fine adjustments of optical components, the spectrometer was ready for measurements.

During spectroscopic investigations the on/off modulation scheme was used for expected strong lines, which could be detected directly. In other cases this scheme was occasionally used, just to verify the presence of TFIR during experiments. For measurements on weak lines frequency modulation has been applied many times, as described in Sect.2.2.3. The lock-in amplifier connected to the bolometer was then tuned to the second harmonic of the modulation frequency. For paramagnetic species Zeeman modulation has been applied via a coil wrapped around the absorption cell (see Sect.3.1 and 3.3.1). The lock-in amplifier was then tuned to the modulation frequency.

2.5.4 Sensitivity of the spectrometer

The power of TFIR generated by the mixer has been determined by comparison with the power level obtained with a crossed-waveguide type mixer of Bičanić (BIC 78), and by reference to specified responsivities of a Golay-type detector and the bolometer in use. It is not possible to give an exact value for power level, because it depends on power of laser and klystron at required frequencies. A typical value of power with the strongest line of the HCN laser was 1 µW, which exceeds the power level of Bičanić's crossed-waveguide mixer by one order of magnitude. This value refers to "normal" microwave power

levels, and could be raised by, say, a factor of five in case of powerful klystrons. It should be noted that the power level of the klystrons was kept below the point of saturation of the diode, because of increasing risk of burn-out. Saturation by laser power was not possible with the lasers in use, and power of TFIR was proportional to laser power. Furthermore, the value of 1 μW is referred to the mixer and has been calculated from the bolometer signal, taking into account losses at optical components between mixer and bolometer window (two lenses, two mirrors, diplexer and monochromator). At 0.9 THz power diminished by a factor of four after traversal of this path.

Although the power detected with the bolometer at 2.5 THz was lower by a factor of hundred when compared to the power at 0.9 THz, it indicated comparable efficiency of the mixer for generation of TFIR. Fundamental power of the water vapour laser was lower than that of the HCN laser by a factor of ten, whereas power losses between mixer and detector were larger by another factor of ten. Enhanced absorption of radiation by polyethylene and by air were responsible for higher losses at 2.5 THz.

Sensitivity of the spectrometer is directly related to power of generated TFIR, because the bolometer determines the noise level under normal conditions. With 1 μW of TFIR (at the mixer) the smallest observable absorption signal at 0.9 THz is equivalent to an absorption of about 10^{-4} of generated TFIR, at an integration time of 0.3 s. Usually a single pass absorption cell of 100 cm length has been used, and sensitivity can be expressed by the minimal observable absorption coefficient

$$\gamma_{min} \simeq 10^{-6} \ cm^{-1} \ .$$

In case of frequency modulation this value really represents ultimate sensitivity, because frequency modulation occasionally produces strong base-line fluctuations. However, sensitivity of $3 \times 10^{-7} \ cm^{-1}$ was obtained using ten times larger integration time in case of straight base-line, usually obtained with Zeeman modulation.

MOLECULAR SPECTRA

3.1 Introduction

Because of its rather peculiar spectral range of operation and
its high resolution, the spectrometer described in the previous
chapter is very well suited for detection and study of rotational
transtions of molecules, including fine- and hyperfine effects.
The following radicals have been studied in the ground
electronic and vibrational state: nitric oxide (NO,$^2\Pi$),
hydroxyl (OD,$^2\Pi$), carbon fluoride (CF,$^2\Pi$), and imine (NH,$^3\Sigma$).
The effect of hindered internal motion has been observed in
transitions of ammonia (NH_3), and methyl silane (CH_3SiH_3).
The feasibility of spectroscopy on molecular ions with the
present spectrometer has been proved by observation of the
ions HCO^+, CO^+ and HN_2^+. Detection of a rotational transition of
the deuterium fluoride (DF) molecule at 2600 GHz illustrates
the possibility to extend the spectral range of the spectro-
meter towards higher frequencies.

     The scheme used for detection of molecular resonances
varied from "direct" observation of absorption, frequency
modulation, and Zeeman modulation, as described in Sect.2.5.3.
The direct scheme was used for DF, NH_3, and NO, frequency
modulation for CH_3SiH_3 and the ions, Zeeman modulation for the
radicals. The Zeeman modulation scheme needs some comment. Free
radicals are paramagnetic species and so exhibit linear Zeeman
effect. The energy shift of a magnetic sublevel caused by an
external magnetic field B equals $g\mu_B$ B M, where g is the g-
factor, μ_B the Bohr magneton and M the magnetic quantum number
associated with the component of the total angular momentum
parallel to the field. In the experimental set-up the magnetic
field is parallel to the $\vec{k}$-vector of the beam of far-infrared
radiation, and only transitions of the type $\Delta M = \pm 1$ can be
observed. This means that the frequency shift $\delta\nu$ of a

41

transition between two magnetic sublevels is given by

$$\delta \nu = [(g_u - g_l)\, M \pm g_u]\, \mu_B\, B/h \qquad\qquad (3-1)$$

where g_u and g_l is the g-factor of the upper and lower level, respectively. The $+(-)$ sign corresponds to $\Delta M = +1(-1)$ transitions. In the experimental set-up discrimination between $\Delta M = +1$ or -1 transitions is not possible. Moreover, it is seen from Eq.(3-1) that the Zeeman effect is symmetric, i.e. the frequency shift for positive M states is as large as for negative M states, and has opposite sign. Consequently no modulation can be expected from an alternating magnetic field. In practice this problem was overcome by addition of a DC component to a (sinusoidally) oscillating field, such that the modulating field oscillated between zero and a maximum value. In that case all Zeeman components coincide during time that field is (almost) zero, whereas they are shifted according to Eq.(3-1) during rest of the period of modulation. The strength of the field amplitude has always been chosen such that 50% of all Zeeman components were shifted by an amount at least equal to the line-width of the zero-field absorption line. The g-factors in Eq.(3-1) were calculated from theory (e.g. DOU 55, HEN 57), and ranged from 0.002 $(NO, {}^2\Pi_{3/2}(J=17/2))$ to 2 $(NH, {}^3\Sigma(N=0,J=1))$.

Details of the absorption cell are given in Sect.3.3.1 and 3.4, in connection with the production of radicals and ions, respectively. For detection of chemically stable molecules the cell just consisted of a simple piece of tubing terminated by polyethylene windows.

3.2 Molecules with hindered internal motion

3.2.1 The inversion spectrum of ammonia $(NH_3, v_2=1)$

Ammonia is the simplest example of a molecule with hindered internal motion. The N-atom has two equivalent positions, one "above", the other "below", with respect to the plane of the H-

atoms. These two positions are separated by a potential barrier of about 2000 cm^{-1}. Tunneling through this barrier gives rise to the well known inversion splitting of all rotational levels. For a complete understanding of vibration-inversion-rotation interaction, the inversion and rotation-inversion spectrum in the $v_2=0$ ground state has been investigated extensively, both experimentally (e.g. POY 75) and theoretically (ALI 76). Most experimental data involve inversion transitions of the type $\Delta J=\Delta K=0$ in the microwave range. Analysis of the J,K-dependence of the measured frequencies has led to refinement of theoretical models. Although data can be fitted with reasonable accuracy to semi-empirical formulas or power series expansions in the rotational quantum numbers J and K, it was recognized already in 1947 (NIE 47), that high order interactions should be taken into account in a proper way, especially the interaction between (J,k) and (J, k±3n) rotational levels, which causes a shift of energy levels known as K-type "splitting". A refinement of the theory of K-type splitting was given by Aliev *et al.* (ALI 76).

With the present spectrometer a few inversion transitions of the type $\Delta J=\Delta K=0$ have been detected in the $v_2=1$ excited state of ammonia, 950 cm^{-1} above the ground state. In this state inversion of the molecule is still hindered by the potential barrier of the H-atoms, and at first sight the structure of the inversion spectrum looks similar to that of the $v_2=0$ state. However, the size of the inversion splittings in the $v_2=1$ state is comparable to that of the rotational splittings. Consequently, the effect of inversion motion on the K-type splitting, which is negligible in the ground state, is rather pronounced in the $v_2=1$ state. At the time measurements were started, a thorough investigation of the inversion spectrum in the excited state was hampered by lack of high resolution data. Data concerning the v_2 band of NH_3 from IR-MW two-photon and IR laser-Stark spectroscopy were available (FREU 76, JON 78, SHI 69), but did not allow for a detailed analysis of the inversion spectrum. Present experiment has been limited to recording of four inversion transitions. Many more ($\sim$40) transitions could have been detected with present spectrometer,

but measurements were discontinued in view of recent
achievements of other groups: independently of present
measurements Urban *et al.* investigated the v_2 band of NH_3
with a grating and diode laser spectrometer, and also
measured the $v_2=1$ inversion spectrum with a high frequency
backward-wave oscillator and Fourier transform spectrometer
(URB 80,81). Moreover, Belov *et al.* (BEL 80) interpreted the
inversion and rotation-inversion spectrum and successfully
fitted eighty measured frequencies to their theoretical model
within the experimental accuracy. They determined twenty-nine
molecular parameters of the $v_2=1$ state. The inversion fre-
quencies determined with present spectrometer and those
obtained by Urban *et al.* (URB 80,81) are in good agreement, as
can be seen from Table 3.1.

TABLE 3.1 : Observed frequencies (in MHz) of inversion transitions
of $NH_3(v_2=1)$

J	K	$v_{observed}$ [a]	$v_{observed}$ [b]
7	5	961 885.2	961 884.8
8	6	958 827.9	958 828.1
9	7	959 569.0	959 566.3
10	8	964 060.3	964 060.2

a) Values taken from Urban *et al.* (URB 80); accuracy 1 MHz

b) This work; accuracy 1 MHz

3.2.2 Torsion-rotational transitions of methyl silane (CH_3SiH_3)

In the CH_3SiH_3 molecule, the methyl and silyl group are bound
by a single C-Si bond which, in principle, allows rotation of
the two groups with respect to each other about the C-Si axis.
This motion is hindered by a three-fold potential barrier,
associated with the torque between the two pyramidal parts of

the molecule. In general the motion is composed of vibration and internal rotation of the molecule and is called torsional motion. The motion resembles an (angular) harmonic oscillation in the low torsional states (e.g. v=0), whereas it is an almost free rotation in torsional states well above the barrier. Big challenge in molecular spectroscopy is construction of an adequate theoretical model describing the complex internal motion, which involves also coupling between torsional and normal rotational motion. A result of this coupling is a splitting of rotational energy levels into torsional triplets. Sublevels are labelled by the parameter $\sigma=0,\pm 1$ (GOR 70). In principle detailed information about the shape of the barrier potential can be obtained from the torsional splittings. However, methyl silane is a symmetric top, which normally obeys the rigorous selection rule $\Delta K=0$ for normal electric dipole transitions. This selection rule eliminates the most crucial splittings from the transition frequencies. Consequently, investigation of internal rotation in methyl silane by conventional absorption experiments is very difficult, if not impossible. Several possibilities to solve this problem have been reviewed by Meerts and Ozier (MEE 82a). They conclude that the avoided-crossing molecular beam electric resonance method (MEE 78) is the most adequate solution. In this type of experiments the $\Delta K=0$ selection rule is broken.

Present measurements, recording of a fragment of the dense rotational spectrum of methyl silane, have been carried out in order to provide additional information in a current investigation of torsional motion in CH_3SiH_3 by Meerts and Ozier (MEE 82b). They are developing a quantitative model which describes internal rotation more adequately than previous models (based on power-series expansion of the barrier potential) did. A virtue of present work has been experimental verification of a preliminary model. Meerts combined present far-infrared data with those from microwave ($J\leq 13$, WON 82) and RF (MEE 82a) experiments in a provisional computer fit. Agreement between the observed and best-fit frequencies is excellent, as can be seen from Table 3.2.

TABLE 3.2 : Rotational transitions of CH_3SiH_3 ; v=0,1,2,
J=45←44, ΔK=Δσ=0

(±K , σ)[a]	$\nu_{observed}$[b]	$\nu_{obs.}-\nu_{calc.}$[c]
v=0 (2,)[a]	983 302.1	0.0
(3,)	983 281.8	-0.0
(4,)	983 252.2	-1.0
(5,)	983 215.4	-1.2
(6,)	983 171.2	-0.8
(7,)	983 119.2	0.1
(8,)	983 058.2	0.2
(9,)	982 989.4	0.7
(10,)	982 912.1	0.3
(11,)	982 826.8	-0.0
(12,)	982 733.4	-0.3
(13,)	982 631.5	-0.7
(19,)	981 855.5	-0.0
(20,)	981 698.6	0.1
v=1 (0, 0)	980 439.8	2.2
(0, ±1),(2, 0),(3, ±1)	980 403.8	
(1, 0)	980 429.4	1.0
(1, ±1),(2, ±1)	980 417.1	
(1, ∓1)	980 392.1	-1.0
(2, ∓1)	980 380.1	-0.8
(3, 0),(3, ∓1),(4, ±1)	980 368.5	
(4, 0),(5, ∓1)	980 331.5	
(4, ∓1)	980 355.7	0.4
(5, 0),(6, ∓1)	980 294.0	
(5, ±1)	980 317.4	0.5
(6, 0),(6, ±1)	980 259.3	
(7, 0)	980 220.9	0.2
(7, ±1)	980 194.7	-1.1
(7, ∓1)	980 231.9	0.5
(8, 0)	980 172.4	0.4

(cont'd)

46

	(8, ± 1)	980 135.4	0.3
	(8, ∓ 1)	980 156.6	-0.1
	(9, 0)	980 107.7	1.0
	(9, ± 1),(9, ∓ 1)	980 073.9	
	(10, 0)	980 023.4	0.7
	(10,± 1)	980 013.3	0.5
	(10,∓ 1)	979 986.2	-0.4
v=2	(0, 0)	977 570.4	1.4
	(0, ± 1)	977 827.3	-0.3
	(1, 0)	977 596.2	0.1
	(1, ± 1)	977 691.2	-0.5
	(1, ∓ 1)	977 934.7	0.6
	(2, 0)	977 674.5	-1.3
	(2, ∓ 1)	977 921.4	0.3
	(3, 0),(3, ∓ 1)	977 790.2	
	(3, ± 1),(4, ± 1)	977 530.6	
	(4, 0)	977 875.8	-0.1
	(4, ∓ 1)	977 633.1	0.3
	(5, 0)	977 836.5	0.0
	(6, 0),(8, ± 1)	977 681.5	
	(7, ± 1)	977 745.0	-1.6
	(13,± 1),(14,± 1)	976 877.9	
	(15, 0)	976 912.3	-0.1

a) Upper sign of σ corresponds to positive, lower to negative K-value. Torsional structure in the ground state (v=0) not resolved.

b) Frequencies given in MHz; experimental accuracy 1 MHz.

c) Result of provisional analysis; overlapping lines were left out of computer fit.

It should be noted that the absolute frequencies of the lines were predictable only with an accuracy of about 800 MHz before measurements were started.

Deformation of the pyramidal structure of the methyl and silyl group by centrifugal forces is considerable. Consequently, high order effects associated with centrifugal distortion, like the torsional dependence of the rotational constant A, are rather pronounced. Prediction of electric field strength and transition frequencies in avoided-crossing experiments is very sensitive to these effects. Present recording of rotational transitions of the type $\Delta J=1$, $\Delta K=\Delta\sigma=0$ in the torsional states $v=0,1,2$ provided values of three centrifugal distortion parameters. This complementary information will be used in forthcoming avoided-crossing experiments by Meerts and Ozier (MEE 82b).

3.3 Free radicals

3.3.1 Production

When a beam of radiation passes through a cell containing a weakly absorbing medium, the amount of power absorbed by the medium is proportional to the product of the volume density n of resonant molecules and the path-length l of the cell. In order to make this product as large as possible, a 1 m long absorption cell has been constructed containing two electrodes for an internal DC glow discharge over its full length. When the cell contains the proper gas or mixture of gases, a dis- charge constitutes an efficient source for production of radicals. In view of high chemical activity of radicals in a cell and the resulting short life-time, an internal discharge guarantees a constant supply of radicals over full extent of the cell.

Constructional details of the cell are illustrated in Fig. 10. It consists of a glass tube, approximately as wide as the beams of far-infrared radiation in use (5.5 cm), terminated by polyethylene windows. A stainless steel anode ring and a
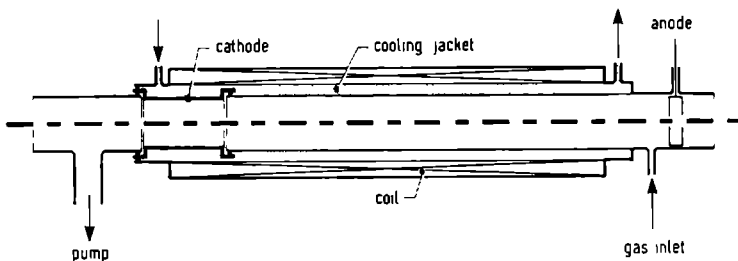
Fig.10 : Absorption cell with internal discharge.

gas inlet are placed at one end, a stainless steel cathode and
a pumping port at the other end. The cylindrical 10 cm long
cathode is incorporated as part of the cell wall. Cathode and
major part of the cell are cooled by a constant flow of water
through a jacket. The discharge is maintained by a voltage
regulated power supply at voltages and currents typically
below 2.5 kV and 0.5 A, respectively. Constant refreshment of
the discharge medium is assured by a fast gas flow, maintained
by a rotary pump (16 m^3/h) backed up by a liquid nitrogen trap.
Typical pressure inside the cell is in the range 1-15 Pa.

   Since radicals are paramagnetic, Zeeman modulation is
applicable. The modulation field is produced by a coil wrapped
around the absorption cell. The coil has a length of 1 m and
produces a biased alternating magnetic field, directed along
the axis of the cell (cf. Sect.3.1). The coil is part of two
electrical circuits. For an AC current the coil is combined
in series with a condensor to an LC-circuit, resonant at the
modulation frequency and fed by an AC oscillator and a 100 W
power amplifier. The bias current is supplied by a DC power
supply. Both circuits are isolated from each other by a
condensor and a choke, in order to prevent feedback and damage
to the power supplies. With this coil a magnetic field could
be obtained that oscillated sinusoidally between zero and 20
mT. The upper limit of the field was set by the power supplies.

3.3.2 Rotational spectrum of ^{14}NO and ^{15}NO

Nitric oxide (NO) is a stable molecule and so not a free
radical from a chemical point of view. However, the nitric
oxide molecule has an open-shell electronic configuration, the
property shared with all chemical free radicals. The electronic
ground state is $^2\Pi_\Omega(\Omega=1/2,3/2)$.

Part of the rotational spectrum of the normal isotope
(^{14}NO) has been recorded with the far-infrared spectrometer
using pure NO gas from a container. The Λ-doubling of
rotational lines was resolved easily, both in the $^2\Pi_{1/2}$ and
$^2\Pi_{3/2}$ electronic state. Usually, molecular resonances were
detected by "direct observation of absorption" (on/off
modulation of incident radiation). The far-infrared frequencies
obtained have been combined with results of high resolution
studies in the infrared, microwave and RF region. Excellent
consistency of all data was found in a least-squares fit,
resulting in improved accuracy of rotational and Λ-doubling
constants. For a detailed description of experiment and spectrum
analysis, the reader is referred to paper no.1 of this thesis
(HEU 80). The NO experiment clearly demonstrates the suitability
of the spectrometer for investigation of spectra in a considerable
frequency range (200-300 GHz) around the HCN laser lines.

The ^{14}NO molecule has also been used to test both the
production of molecules in a discharge and spectrometer
sensitivity. Production of ^{14}NO in a discharge through normal
air was tried, while the spectrometer was tuned to a resonance
frequency determined in earlier experiments with pure NO gas.
The absorption cell described in Sect.3.3.1 was used for this
purpose. The $^2\Pi_{3/2}$, J=19/2 + 17/2 rotational Λ-doublet at 979
GHz was easily observed in a 250 mA discharge through fast
flowing air at a total pressure of about 50 Pa. Zeeman modulation
was applied and signal to noise (S/N) ratio was about 40 at
RC=1 s. It is worthwhile to note that presence of NO radicals
in a discharge through air is not self-evident. In a separate
experiment it was observed that NO molecules are destroyed very

efficiently by a single pulse of current struck through pure
nitric oxide gas.

The ^{15}NO species of nitric oxide was used to test sensiti-
vity of the spectrometer. In a natural sample of nitric oxide
gas, absorption lines have been recorded at 944 and 1042 GHz,
corresponding to the J=19/2 ← 17/2 and J=21/2 ← 19/2 rotational
transitions of ^{15}NO in its $^2\Pi_{3/2}$ electronic state. Despite the
low natural abundance of ^{15}NO(0.37%) and its small electric
dipole moment (0.5×10^{-30} Cm), the S/N ratio was about 60 at
RC=1 s. The observed frequencies, given in Table 3.3, are in

TABLE 3.3 : Rotational transitions of ^{15}NO(X$^2\Pi_{3/2}$(v=0))

Identification[a]		$\nu_{observed}$[b]	$\nu_{obs.} - \nu_{calc.}$[c]
J+1 ← J	parity change		
19/2 ← 17/2	− ← +	943 760.8	−0.5
19/2 ← 17/2	+ ← −	943 795.0	−0.7
21/2 ← 19/2	+ ← −	1042 874.2	0.7

a) Hyperfine structure was not resolved

b) Frequencies given in MHz; experimental accuracy 1 MHz

c) Accuracy of prediction 1.4 MHz

accordance with predicted values from a computer analysis based
on infrared, microwave and molecular beam electric resonance
studies (AMI 79, GAL 56, MEE 72).

3.3.3   The J=3/2 ← 1/2 transition of OD

The OD radical ($^2\Pi$ electronic ground state) is relatively stable
and can be produced easily. Its UV spectrum was recorded in a
hollow cathode discharge through heavy water vapour (D$_2$O) by
Carlone *et al.* (CAR 69). The cell described in Sect.3.3.1
offers a similar method of production. The J=3/2 ← 1/2

rotational transition of the radical in its $^2\Pi_{1/2}$ electronic
and vibrational ground state has been observed at 944 GHz. A
recording is reproduced in Fig.11. Signal to noise ratio   is
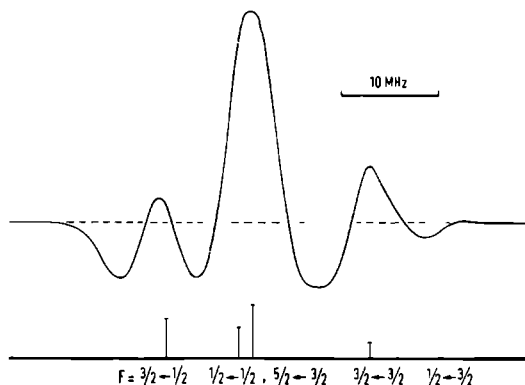
Fig.11 : Hyperfine structure of the J=3/2←1/2 rotational transition of
the OD radical in the $^2\Pi_{1/2}$ ground state. Only one of the Λ-
components is shown. Amplitude of Zeeman modulation field 4 mT.

in the order of 1000 at RC=1 s. Only the upper Λ-doubling
levels of both the upper and lower rotational level are
involved in the recorded transition. The satellite line
originating from a transition between the lower Λ-doubling
levels was predicted at a frequency of 941.4(4) GHz (CLY 73).
Unfortunately this line could not be observed, because the
required klystron with a frequency of 50 GHz was not available.
Structure of the absorpion line at 944 GHz is caused by
hyperfine interactions and permits unambiguous identification
of the molecular resonance as due to the OD radical. The
observed structure fits very well to prediction based on a
molecular beam electric resonance study of the hyperfine
structure by Meerts and Dymanus (MEE 73). Both the predicted
hyperfine splittings and the predicted relative intensities
are presented in Fig.11. The intensities have been calculated
using formulas given by ter Meulen (MEU 76). It should be
noted that the recorded intensities in Fig.11 are slightly
destorted by overlap of Zeeman components. The observed

frequencies given in Table 3.4 have been used by Brown *et al.*
(BRO 82) in an analysis of electron paramagnetic and laser
magnetic resonance data. It can be seen from Table 3.4 that

TABLE 3.4 : Frequencies corresponding to one of the Λ-doubling components[a]
of the J=3/2$\leftarrow$1/2 rotational transition of OD ($X^2\Pi_{1/2}$(v=0))

F'	$\leftarrow$	F	$\nu_{observed}$[b]	$\nu_{obs.} - \nu_{calc.}$[c]
3/2		3/2	944 412.0	-0.9
5/2		3/2 }	944 424.4	{ -0.5
1/2		1/2		-2.0
3/2		1/2	944 433.3	-0.5

a) See text

b) Frequencies given in MHz; experimental accuracy 1 MHz

c) Combined analysis with LMR- and EPR-data (BRO 82)

the deviation of the observed frequencies from the best-fit
values is within the experimental limit of accuracy, indicating
consistency of present data with the other data used in the
analysis of Brown *et al.*

The concentration n of OD radicals has been calculated
from the observed absorption intensity, making use of a well-
known formula (TOW 55) for the absorption coefficient γ

$$\gamma = (8\pi^2/3 \ c \ k \ T) \ f \ n \ <\mu>^2 \ \nu_0^2/\Delta\nu \tag{3-2}$$

with T the rotational temperature (estimated at 500°K), f the
fraction of OD radicals in the lower level involved in the
transition (1.5%), $<\mu>$ the dipole moment matrix element (4×10^{-30}
Cm), ν_0 the transition frequency, and $\Delta\nu$ the halfwidth of the
absorption line (2.3 MHz). This calculation yields for the
concentration 7×10^{12} cm^{-3}, which is equivalent to an OD partial

pressure of 2.5×10^{-2} Pa. Fraction of OD molecules in the cell
is 0.25%, while concentration of molecules involved in a
single hyperfine rotational transition (=fn) is equivalent
to a partial pressure of 4×10^{-4} Pa.

3.3.4 Rotational spectrum of CF

The rotational spectrum of CF is quite similar to that of
isoelectronic nitric oxide. Although the radical has been
observed in various parts of the electromagnetic spectrum
(UV, infrared, microwave and RF), it has not been possible to
determine all four hyperfine constants of Frosch and Foley
(FRO 52) and one of the Λ-doubling parameters. Investigation
of the radical with the present spectrometer was undertaken
in order to determine these constants.

The CF radical is produced most often by an electro-
deless microwave discharge through CF_4, C_2F_4 or C_4F_8, either
pure or mixed with argon. Sometimes secondary gases are added to
the discharge medium to capture free fluorine atoms. In
present experiments first signals were indeed observed using
a microwave discharge through CF_4 and argon for production.
However, CF was produced more successfully in a glow
discharge through a critical mixture of CF_4, argon and CH_3F
in the cell described in Sect.3.3.1. After a few hours of
operation decomposites were visibly present on the wall of the
cell and addition of CH_3F to the gas mixture was reduced in
order to prevent diminution of absorption intensity. Obviously
the role of CH_3F in the discharge chemistry was taken over by
the decomposites.

Seven rotational transitions of CF in the $^2\Pi(\Omega=1/2, 3/2)$
ground state were detected; one of them is shown in Fig.12
with fully resolved Λ-doubling and hyperfine structure. The
experimental results and analysis are described in detail in
paper no. 2 of this thesis (HEU 82).
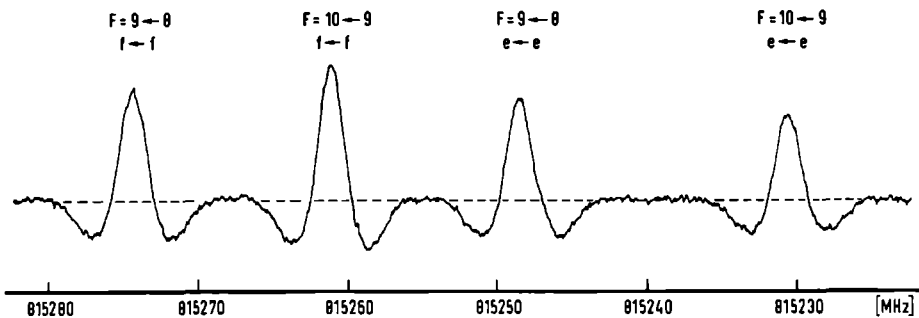
Figure 12 : *Λ-doubling and hyperfine structure of the J=19/2 ← 17/2 rotational transition of the CF radical in the $^2\Pi_{3/2}$ ground state. For this transition the label e(f) corresponds to the lower (upper) Λ-doubling level.*
Amplitude of Zeeman modulation field 5 mT.

Rotational hyperfine spectrum of the NH radical around 1 THz

F.C. van den Heuvel, W.Leo Meerts and A. Dymanus,

Katholieke Universiteit, Fysisch Laboratorium, 6525 ED Nijmegen,

The Netherlands

Abstract

The rotational transitions $N = 1 \leftarrow 0$, $J = 2 \leftarrow 1$ and $N = 1 \leftarrow 0$, $J = 1 \leftarrow 1$ of the NH radical in the $^3\Sigma^-$ electronic and vibrational ground state have been observed around 1 THz with resolved hyperfine structure. Spectra were recorded at zero magnetic field, using a tunable laser-sideband spectrometer. Analysis yielded improved values of the magnetic hyperfine parameters and the rotational constants.

Introduction

For a long time the rotational spectrum of the NH radical has been inaccessible to high resolution spectroscopy, because the spectrum lies beyond the frequency range of conventional microwave spectrometers. A few years ago the radical was studied with the technique of laser magnetic resonance (LMR), (1). These investigations permitted the first determination of the Frosch and Foley (2) magnetic hyperfine parameters b and c, for both the nitrogen and hydrogen nucleus. The experiments demonstrated power of the LMR technique in the far-infrared region, in particular with respect to sensitivity. However, with the LMR technique molecular zero-field constants are deduced from a fit of (generally) complex magnetic spectra, which also depend on first and second order Zeeman parameters. These features and field inhomogeneities often limit accuracy of the constants derived. In this communication we report of the pure (zero-field) rotational spectrum of the normal species ^{14}NH in the ground electronic and vibrational state $X^3\Sigma^-$, $v = 0$. The transitions $N = 1 \leftarrow 0$, $J = 2 \leftarrow 1$ and $N = 1 \leftarrow 0$, $J = 1 \leftarrow 1$ have been recorded with the spectrometer used for the successful investigation of the CF radical (3).

Experimental details

Tunable far-infrared radiation has been produced by mixing the radiation of a hydrogen cyanide discharge laser (frequency 890.7603 GHz) with that of a klystron, using a Schottky barrier diode as non-linear element. An outline of the spectrometer has been given elsewhere (3). The frequencies required for present experiments, 974 GHz ($J = 2 \leftarrow 1$) and 1000 GHz ($J = 1 \leftarrow 1$), were obtained with klystrons operating at 83 and 109 GHz, respectively.

The method of producing NH radicals was different from the one

applied in LMR studies (1). Instead of repetitive hydrogen abstraction

from ammonia by fluorine atoms (produced in a microwave discharge through

CF_4), a DC glow discharge through pure ammonia was chosen for production.

Discharge was struck in a water cooled 1 m long cell with a diameter of

5 cm. Strongest absorption signals were observed at a discharge current

of about 200 mA with a signal-to-noise ratio of about 50 at RC = 1s. A

recording is reproduced in Fig. 1. Total pressure of the continuously

flowing discharge medium was 25 Pa. Zeeman modulation has been applied

for detection. A coil wrapped around the cell produced a biased magnetic

field that oscillated sinusoidally between 0 - 0.7 mT.

While searching for NH an unexpected line was recorded which could

originate neither from a paramagnetic species nor from the ammonia molecule.

The resonance appeared at 974 488.4(8) GHz, at a distance of only few

MHz from the hyperfine-free frequency of the J = 2 ← 1 transition of NH.

Observation of the line was prohibited using Zeeman modulation, but

absorption was clearly visible by monitoring the power of laser-sideband

radiation. At low pressure of the order of 1 Pa absorption intensity was

equal to 100%. The line was identified as the J = 11 ← 10 rotational

transition of the hydrogen cyanide (HCN) molecule. Probably the molecule

has been produced at low pressure in presence of carbon atoms sputtered

from the electrodes. It is very well possible that the presence of carbon

atoms has been detrimental to NH production efficiency.

Analysis and Results

The effective Hamiltonian is composed of a rotational and rotational

fine structure term, a term associated with magnetic hyperfine interactions

and a quadrupole term:

$$H = H_{Rfs} + H_{mhf} + H_Q$$

In case of NH, the rotational levels with $\Delta N = \pm 1$ are separated by at least 950 GHz, the $N = 1$ ($J = 0$, 1, 2) fine structure levels by 25-30 GHz, which is large compared to the hyperfine splittings ($\leqslant 0.085$ GHz). Consequently, the hyperfine and rotational fine structure have been analyzed separately: hyperfine interaction can be treated as a small perturbation on the widely spaced rotational (N, J) levels. We used the explicit formulas of Miller and Townes (4) to describe the pure rotational spectrum, including fine structure effects. These formulas contain the rotational constant (B), the spin-spin constant (λ) and the spin-rotation constant (γ). An expression for the magnetic hyperfine term H_{mhf} was derived by Frosh and Foley (2). These authors introduced the magnetic hyperfine parameters b and c. We used the tensorial form of their Hamiltonian, which was given by Wayne and Radford (1b).

Calculation of the hyperfine matrix elements has been performed in the representation $| NSJI_1F_1I_2FM_F >$ corresponding to the coupling scheme $\vec{J} = \vec{N} + \vec{S}$, $\vec{F}_1 = \vec{J} + \vec{I}_1$, $\vec{F} = \vec{F}_1 + \vec{I}_2$. Matrix elements of the type $<N'SJ'I_1F_1'I_2F'M_F' | (H_{mhf} + H_Q) | NSJI_1F_1I_2FM_F >$ were calculated with the aid of spherical tensor methods (5). Explicit formulas can be found elsewhere (6). The number J is an approximately good quantum number. We estimated by second order perturbation calculation that the effects of matrix elements of the type $\Delta J = 0$, $\Delta N \neq 0$ and of the type $\Delta J \neq 0$ are smaller than 0.01 MHz and 0.3 MHz, respectively. As the full Doppler linewidth is 5 MHz, contributions from these matrix elements can be neglected.

As a first step we compared our recorded spectra with prediction based on the four hyperfine constants (b_H, c_H, b_N, c_N) determined by Wayne and Radford (1b). Like these authors we neglected the small influence of the quadrupole interaction term in the hamiltonian at this stage.

The calculated and observed spectra showed resemblance, but many lines
were shifted by an amount close to or slightly beyond the limits set
by the accuracy of the constants (we allowed the constants to vary within
their quoted error limits). Although the calculated spectra facilitated
identification of the observed lines, some parts of the recordings
consisted of closely spaces, sometimes unresolved lines. Relative intensities
have been calculated in order to make identifications unambiguous. Dipole
moment matrix elements were calculated with standard formulas (7), using
the eigenfunctions of the hyperfine Hamiltonian. In a preliminary fit we
included only the frequencies corresponding to the center of singular
absorption lines and obtained the position of lines that were not yet
included in the fit. In case of closely spaced lines we weighted the
frequencies according to intensity and calculated the centre of the
composite line corresponding to such a cluster. In this way we were
able to take into the fit the frequencies of four observed composite
lines. The procedure converged by iteration to the final fit, in which
we included 14 experimental frequencies and determined the four hyperfine
parameters. Like in the previous fits, the positions of the two centra of
the rotational $J = 2 \leftarrow 1$ and $J = 1 \leftarrow 1$ hyperfine spectra were regarded
as floating parameters. Consequently the final fit yielded both the
hyperfine constants and the following hyperfine-free rotational
frequencies:

$$\nu_0 \ (J = 2 \leftarrow 1) = 974\ 474.85(80)\ \text{MHz}$$
$$\nu_0 \ (J = 1 \leftarrow 1) = 999\ 974.03(80)\ \text{MHz}$$

A comparison between observed and best-fit spectra is presented in
Table 1, the best-fit hyperfine constants are given in Table 2. Inclusion
of the quadrupole term in the Hamiltonian neither improved the fit, nor
yielded a significant value for eqQ. Therefore this term was left out

of the final fit. The values of our hyperfine parameters and those

obtained by Wayne and Radford (1b) are in good agreement within two

standard deviations. Our analysis confirms the choice made by Wayne and

Radford for the absolute sign of the b and c constants, which they made

in agreement with ab initio calculation.

Above we determined the hyperfine-free frequencies ν_0 corresponding

to the N = 1 ← 0, J = 2 ← 1 and N = 1 ← 0, J = 1 ← 1 transition. A third

transition (N = 1 ← 0, J = 0 ← 1), predicted at 946 GHz, was not searched

for, but even if this transition was recorded as well, the number of ex-

perimental fine structure data would have been insufficient to determine

both the rotational constants B, the fine structure constants λ and γ

and the centrifugal distortion parameter D. However, the values of ν_0

(J = 2 ← 1) and ν_0 (J = 1 ← 1) given above have an accuracy which is much

better than the accuracy of prediction ($\approx$ 15 MHz) based on the values of

B, λ and γ determined by Wayne and Radford (1b) and the value of D of Dixon

(9). We therefore determined the parameters B, D, λ and γ in a least-

squares analysis with our frequencies ν_0, while constraining the

parameters to their known values within the quoted limits of accuracy.

The values of B, λ and γ were taken from Ref. (1b), the value D =

17.14(3) x 10^{-4} cm^{-1} from Bollmark et al (8). As part of their investi-

gation the latter authors reanalyzed the optical spectra obtained by

Dixon (9). We followed the method of Bollmark et al to introduce the

centrifugal distortion parameter D in the formulas of Miller and Townes.

The fit yielded the values of the parameters given in Table 2. The accuracy

of the value of B is significantly improved.

Concluding remarks

The current work demonstrates the capability of a far-infrared laser-

sideband spectrometer to obtain high resolution spectra of light

radicals which can not be studied in the microwave region. The laser-

sideband spectrometer may become a serious competitor of the LMR technique

which is the only powerful method in the far-infrared up till now to

study radicals and ions. The present spectrometer can be used to study non-

magnetic molecules and states and produces spectra at zero magnetic field .

Recently (10), for example, we obtained rotational spectra of ions in the

ground electronic and vibrational state: HCO^+ ($^1\Sigma$) and HN_2^+ ($^1\Sigma$).

References

(1) a. H.E. Radford and M.M. Litvak, Chem. Phys. Lett. $\underline{34}$ (1975) 561

b. F.D. Wayne and H.E. Radford, Mol. Phys. $\underline{32}$ (1976) 1407

(2) R.A. Frosch and H.M. Foley, Phys. Rev. $\underline{88}$ (1952) 1337

(3) F.C. van den Heuvel, W.L. Meerts and A. Dymanus, Chem Phys. Lett. $\underline{88}$ (1982) 59

(4) S.L. Miller and C.H. Townes, Phys. Rev. $\underline{90}$ (1953) 537

(5) A.R. Edmonds, "Angular momentum in quantum mechanics", Princeton University Press, New Yersey (1957)

(6) F.C. van den Heuvel, Ph.D. Thesis, Katholieke Universiteit Nijmegen, The Netherlands (1982)

(7) W. Gordy and R.L. Cook, "Microwave molecular spectroscopy", Interscience Publ. Inc.,New York (1970),p. 300

(8) P. Bollmark, I. Kopp and B. Rydh, J. Mol. Spectrosc. $\underline{34}$ (1970) 487

(9) R.N. Dixon, Can. J. Phys. $\underline{37}$ (1959) 1171

(10) F.C. van den Heuvel, and A. Dymanus, to be published (1982)

Identification [a]		$\nu_{obs.} - \nu_0$ [b]	$\nu_{obs.} - \nu_{calc.}$
ΔF	F		
J = 2 ← 1 1	5/2, 3/2, 1/2	3.47(80)	0.22
1	3/2	-4.26(40)	-0.44
1	1/2	-12.99(40)	0.50
0	5/2, 3/2	-38.28(60)	-0.34
0	1/2	-24.53(150)	0.42
J = 1 ← 1 1,0	3/2	34.97(60)	0.43
1	1/2	-52.94(60)	-0.35
1	1/2	-28.97(40)	-0.07
0	5/2	-0.62(40)	-0.20
0	3/2	60.27(60)	0.24
0,1	1/2	79.94(120)	0.45
-1	5/2	26.41(40)	0.03
-1	3/2	-66.11(60)	0.52
-1	3/2	72.35(120)	-1.54

a) The F value is given for the lower (N = 0, J = 1) level; note that the total F momentum may have different (F_1, I_2) parentages. A line with more than one identification consisted of overlapping hyperfine components and was treated as described in the text.

b) Position of the lines in MHz referred to the centra of the hyperfine spectra. Values of the hyperfine-free rotational frequencies ν_0(J = 2 ← 1) and ν_0 (J = 1 ← 1) are given in the text.

Table 2 Molecular parameters of NH (in MHz)

	This work	Ref. 1b
B [a]	489 959.26(68)	489 960(6)
λ	27 581.1(43)	27 572(6)
γ	-1642.4(17)	-1638.7(24)
b_H	-96.80(57)	-100.2(26)
c_H	91.70(160)	88.8(48)
$b_H + c_H/3$	-66.23(32)	-70.6(10)
b_N	41.86(33)	42.8(16)
c_N	-67.94(61)	-68.4(30)
$b_N + c_N/3$	19.22(18)	20.0(6)

a) In this work the distortion parameter D was constrained to the value 51.384(90) MHz (Ref. 8), while it was held fixed to 16.85×10^{-4} cm^{-1} (50.515 MHz, Ref. (9)), in Ref. 1b.
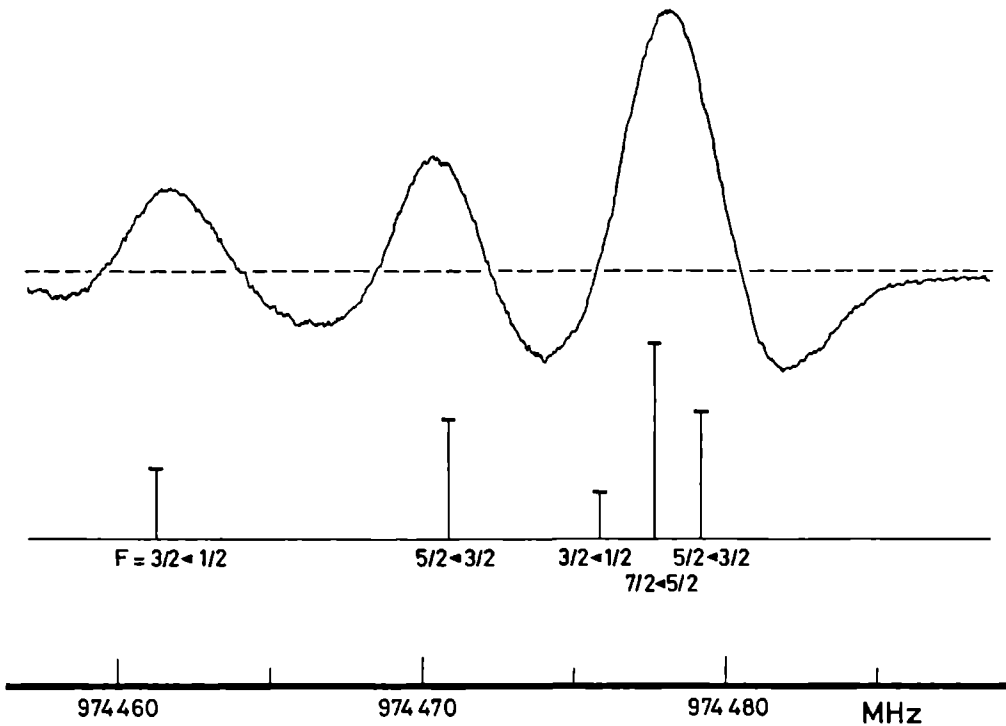
Fig. 1

Central part of the N = 1 ← 0, J = 2 ← 1 rotational hyperfine spectrum recorded at 974 GHz and the best-fit spectrum with the relative intensities.

APPENDIX

The hamiltonian which describes the hyperfine interactions in a molecule in an electronic $^3\Sigma$ state can be split into a magnetic part associated with the dipole-dipole interaction between nuclear and electron spins, and a term associated with the electric quadrupole interaction between nuclei and orbiting electrons. An expression for the magnetic part was derived by Frosch and Foley (FRO 52) and rewritten in irreducible tensor form by Carrington et $al.$ (CAR 67). For analysis of the NH spectra obtained with the laser-sideband spectrometer we applied the hamiltonian which Wayne and Radford (WAY 76) used to interpret their laser magnetic resonance spectra of NH:

$$H_{hf}= \sum_{k} (H_{m1,k}+H_{m2,k}+H_{Q,k})$$

where the index k runs over the nuclei; $H_{m1,k}$ represents the Fermi-contact term

$$H_{m1,k}=(b_k+c_k/3)\ I_k^{(1)}.S^{(1)}\ ,$$

$H_{m2,k}$ the dipole-dipole interaction (partially contained in $H_{m1,k}$')

$$H_{m2,k}=-\sqrt{10}(c_k/3)\ I_k^{(1)}.T^{(1)}(S^{(1)},C^{(2)}(\omega))\ ,$$

and $H_{Q,k}$ the quadrupole interaction

$$H_{Q,k}=\sqrt{(3/2)}\ eqQ_k\ [2I_k(2I_k-1)]^{-1}\ C^{(2)}(\omega).T^{(2)}(I_k^{(1)},I_k^{(1)})\ ;$$

The constants b_k and c_k are the hyperfine parameters of Frosch and Foley.

The hyperfine matrix has been constructed in the $|NSJI_1F_1I_2FM_F>$ representation corresponding to the coupling scheme $\vec{J}=\vec{N}+\vec{S}$, $\vec{F_1}=\vec{J}+\vec{I_1}$, $\vec{F}=\vec{F_1}+\vec{I_2}$. Matrix elements were calculated explicitly by Carrington et $al.$ (CAR 67) for a

diatomic molecule with a single nuclear spin (^{33}SO($X^3\Sigma$)) and by Freund *et al.* (FRE 70) for a diatomic homonuclear molecule (N_2($A^3\Sigma$)). Matrix elements were calculated in an analogous way for the NH radical ($I_H=1/2$ and $I_N=1$), with the aid of spherical tensor techniques (EDM 57, JUD 63).

The hyperfine matrix is diagonal in F and M_F:

$$<NSJI_1F_1'I_2F'M_F'|H_{hf}|NSJI_1F_1I_2FM_F>=\delta(F',F)\,\delta(M_F',M_F)\ <H_{hf}>$$

$$<H_{m1,k}>=(-1)^{e_{m1}}(2J+1)\,[S(S+1)(2S+1)]^{\frac{1}{2}}\begin{Bmatrix}J&J&1\\S&S&N\end{Bmatrix}g_k\,h_{m1}(I_k)$$

$$<H_{m2,k}>=(-1)^{e_{m2}}(2J+1)(2N+1)[30\ S(S+1)(2S+1)]^{\frac{1}{2}}$$

$$\times\begin{pmatrix}N&2&N\\0&0&0\end{pmatrix}\begin{Bmatrix}J&J&1\\S&S&1\\N&N&2\end{Bmatrix}g_k\,h_{m2}(I_k)$$

$$<H_{Q,k}>=(-1)^{e_Q}(2J+1)(2N+1)\begin{pmatrix}N&2&N\\0&0&0\end{pmatrix}\begin{Bmatrix}J&J&2\\N&N&S\end{Bmatrix}g_k\,h_Q(I_k)$$

(The index k indicates whether the hamiltonians operate on the first nuclear spin (I_1) or on the second (I_2)) with

$$e_{m1}=N+S+2J+I_1+I_2+F$$

$$e_{m2}=N+2S+3J+I_1+I_2+F$$

$$e_Q=1+S+2J+I_1+I_2+F$$

and

$$g_1=\delta(F_1',F_1)(-1)^{3F_1+I_2+F+1}\begin{Bmatrix}J&J&1\\I_1&I_1&F_1\end{Bmatrix}$$

$$g_2=(-1)^{2F_1'}[(2F_1'+1)(2F_1+1)]^{\frac{1}{2}}\begin{Bmatrix}F_1'&F_1&1\\J&J&I_1\end{Bmatrix}\begin{Bmatrix}F_1'&F_1&1\\I_2&I_2&F\end{Bmatrix}$$

and

$$h_{m1}(I_k) = [I_k(I_k+1)(2I_k+1)]^{\frac{1}{2}} (b_k+c_k/3)$$

$$h_{m2}(I_k) = [I_k(I_k+1)(2I_k+1)]^{\frac{1}{2}} (c_k/3)$$

$$h_Q(I_k) = [(2I_k+1)(2I_k+2)(2I_k+3)]^{\frac{1}{2}} [2I_k(2I_k-1)]^{-\frac{1}{2}} eqQ_k/2$$

For a complete analysis of the NH spectrum also relative line intensities were needed. As a first step, dipole moment matrix elements have been calculated in the $|NSJI_1F_1I_2FM_F>$ representation, again with spherical tensor methods. In order to obtain the actual intensities, dipole moment matrix elements of the type $<upper|\vec{\mu}|lower>$ were calculated, using the eigenfunctions of the hyperfine hamiltonian H_{hf} :

$$|upper> \equiv |N',J',F'> = \sum_i a_i' |N'SJ'I_1F_{1i}'I_2F'>$$

$$|lower> \equiv |N, J, F> = \sum_j a_j |N SJ I_1F_{1j}I_2F>$$

The coefficients a_i',a_j were determined by diagonalization of the hyperfine matrix. In the analysis N'=1 and N=0 and only J,F dependence of the intensities was considered. Calculation yielded for the relative intensities:

$$I_{rel}(N'=1,J',F' \leftarrow N=0,J,F) = |C(J',F';J,F)|^2$$

with

$$C(J',F';J,F) = [(2J'+1)(2F'+1)(2J+1)(2F+1)]^{\frac{1}{2}} \begin{Bmatrix} J' & N' & S \\ N & J & 1 \end{Bmatrix}$$

$$\times \sum_{i,j} (-1)^{F'_{1i}+F_{1j}} a'_i a_j [(2F'_{1i}+1)(2F_{1j}+1)]^{\frac{1}{2}}$$

$$\times \begin{Bmatrix} F'_{1i} & J' & I_1 \\ J & F_{1j} & 1 \end{Bmatrix} \begin{Bmatrix} F' & F'_{1i} & I_2 \\ F_{1j} & F & 1 \end{Bmatrix}$$

Observation of far-infrared transitions of HCO^+, CO^+ and HN_2^+

F.C. van den Heuvel and A. Dymanus

Fysisch Laboratorium, Katholieke Universiteit,
6525 ED Nijmegen, The Netherlands

Abstract

Rotational transitions of molecular ions HCO^+, CO^+, and HN_2^+ have been observed at frequencies around 1 THz. The ions were produced in the negative glow of a hollow cathode discharge cooled by liquid nitrogen. Preliminary results indicate efficient production of ions in an absorption cell of simple construction.

In spite of considerable instrumental difficulties spectroscopic investigation of molecular ions receives growing attention in microwave spectroscopy. In a recent article (1) Saykally and Woods have reviewed progress and present state of the art of spectroscopy in the infrared and microwave region. Information derived is complementary to that of spectrometers operating in the visible and ultraviolet region. In this paper the feasibility of molecular ion spectroscopy around 1 THz with high resolution is demonstrated with the observation of three ions of astrophysical importance: HCO^+, CO^+, and HN_2^+. Present results are compared with earlier observations in the microwave range (90-400 GHz). Special attention is payed to the method of ion production and to spectrometer sensitivity.

In Doppler limited spectroscopy a well known and often adequate source for ion production is a glow discharge. In view of collisional destruction of molecular ions, the discharge usually is contained inside the absorption cell, and geometry is chosen such that the product of (average) ion concentration n (cm^{-3}) and pass length l is as large as possible. There are various ways to obtain such a discharge. Satisfactory results have been obtained (2-4) with a DC discharge between electrodes placed at either end of a long glass tube, and with

72

an electrodeless discharge maintained by a high power R.F. oscillator
(5,6). In both methods a beam of microwave radiation traversed the
absorption cell in axial direction, and attenuation of power due to
resonant absorption by ions was spatially averaged over various parts
of the discharge. Temperature of cell walls played an essential role
in production of molecular ions. Absorption signals at liquid nitrogen
temperature were much stronger than at room temperature.

A DC glow discharge is composed of distinct zones, and the spatial
variation of its parameters (potential, field strength, electron speed,
and current density) has strong correlation with these zones (7). The
positive column, which usually fills most of a discharge tube, is known
as a low-field region. In this region current is primarily carried by
electrons, whereas positive ions slowly drift with random movement and
are only present in small concentration. On the other hand, positive
ions are mostly present close to the cathode, especially in and close
to the so-called negative glow, where complex chemical reactions take
place, in the presence of fast electrons and radiation. Mass spectro-
metric investigations (8,9) confirm the pronounced role of the negative
glow region in a DC discharge. Use of the specific properties of the
negative glow has been made by Cossart (10) to obtain emission spectra
of polyatomic ions. He intentionally did not use a hollow cathode
discharge, because of requirements set by the specific application, but
characteristics of the discharge closely resembled those of a hollow
cathode. Cossart also applied liquid nitrogen cooling to the cathode.

2. Experiment and Results

We have tried to combine features that clearly seem to favour
efficient production of molecular ions, in an easy to build absorption

73

cell. It consists of a 0.7 m long copper cathode tube with a diameter

of 50 mm inside a 1 m long glass tube with a diameter of 80 mm. Dis-

charge is struck between the hollow cathode and an anode positioned

at the end of a glass insert of the main tube, as shown in Fig. 1.

Occurrence of the discharge outside the cathode tube is prevented by

teflon seals and a glass tube, inserted between the electrodes. The

cathode can be cooled efficiently by a slow flow of liquid nitrogen

through helical copper tubing soldered around the cathode tube.

Condensation of atmospheric water vapour on the outer cell wall is

absent, because of very small thermal contact with the cold cathode

tube. The discharge strikes easily and stable operation is possible

in a large range of currents and pressures, as expected in a hollow

cathode discharge (10). The positive column is present in the glass

insert between cathode and anode only, and the negative glow concen-

trates along the axis of the cathode tube. At a distance of about 10

mm from the cathode, the glow abruptly changes into the cathode dark

space. The length of the glow is directly related to the voltage applied

to the anode. At low voltages the glow is located near the middle of

the tube, facing the anode, whereas it elongates towards (sometimes

even beyond) the ends of the tube as voltage is increased.

The absorption cell described above, has been used to observe ion

spectra. The basis of the spectrometer is a highly monochromatic source

of far-infrared radiation (11,12), frequency tunable around 30 cm^{-1}. It

produces a wide beam (diameter 4 cm) of radiation that traverses the

single pass absorption cell. Absorption of radiation is directly detected

with a liquid helium cooled bolometer. Rotational transitions of HCO^+,

CO^+, and HN_2^+ have been observed in discharged gas mixtures, composed

of H_2/CO, CO/He, and H_2/N_2, respectively. All gases were of technical

quality and used without additional purification. Fairly fast flow of gases through the cell was maintained by a 16 m^3/h rotary pump, backed up by a liquid nitrogen trap inserted in the pumping line. The discharge was operated at currents up to 300 mA, in such a way that the glow extended over full length of the cathode tube. Further increase of current did not improve absorption intensity substantially. At low cathode temperature all transitions were easily observed (e.g. Fig. 2), but production efficiency went down by at least three orders of magnitude when cooling medium was changed from liquid nitrogen to tap water.

The observed resonant frequencies of the ions in their vibrational ground state are given in Table 1. The transitions have been identified by calculating their frequencies. In case of HCO^+ ($X^1\Sigma$) and HN_2^+ ($X^1\Sigma$) standard formula for $J + 1 \leftarrow J$ transitions was applied. In case of CO^+ ($X^2\Sigma$) the formula

$$\nu = 2B_\bullet (N + 1) - 4D_\bullet (N + 1)^3 - \gamma_0/2$$

was used. The last term takes into account the effect of spin-rotation interaction on the transition frequency in case $\Delta J = \Delta N = 1$ and $J = N - \frac{1}{2}$. ____ With the constants reproduced in Table 2 the agreement between the observed and calculated frequencies is very good.

In case of HCO^+ we estimated the abundance of ions in the absorption cell, using standard formulas (15) relating the absorption coefficient γ with the concentration of HCO^+ ions. From the observed absorption coefficient ($\gamma = 2 \times 10^{-4}$ cm^{-1}) we calculated $n = 3 \times 10^{10}$ cm^{-3}, assuming reasonable values for the translational, rotational, and vibrational temperatures (200, 200, and 1000 °K, respectively), and the electric dipole moment (1.1 $\times$ 10^{-29} Cm, Ref. 16).

3. Conclusions

The experiment described above demonstrates that a cold hollow cathode discharge of simple construction is a very efficient source for ion spectroscopy. Moreover, it shows that very good sensitivity can be achieved with a spectrometer operating beyond the high frequency limit of conventional microwave spectrometers. This stems from the fact that the absorption coefficient γ is proportional to frequency in Doppler limited spectroscopy and that the thermal population of the lowest energy level involved in a rotational transition is more favourable at higher frequencies for an average molecule. For example, in case of HCO^+ the observed value $\gamma = 2 \times 10^{-4}$ cm^{-1} exceeds the value observed by Woods et al (16) by a factor of 200; a factor of 20 can be explained by just these arguments. Finally, the disturbing interaction between a beam of radiation and a discharge plasma that leads to additonial noise or base-line fluctuations at microwave frequencies, is negligible in the far-infrared.

Although temperatures of the cathode tube seems to play an important role in the process of ion formation, it is not clear at the moment whether temperature, or discharge geometry, or the combination of both is responsible for the high yield of ions. Forthcoming investigations might lead to better understanding of chemistry in such a discharge.

References

(1)   R.J. Saykally and R.C. Woods, Ann. Rev. Phys. Chem.
       32, (1981) 403

(2)   T.A. Dixon and R.C. Woods, Phys. Rev. Lett. 34 (1975) 61

(3)   R.C. Woods, Rev. Sci. Instrum. 44 (1973) 282

(4)   K.V.L.N. Sastry, E. Herbst, and F.C. DeLucia
       J. Chem. Phys. 75, (1981) 4169

(5)   M. Bogey, C. DeMuynck, and J.L. Destombes
       Mol. Phys. 43, (1981) 1043

(6)   R. Bustreel, C. DeMuynck, J.L. Destombes, and G. Journel
       Chem. Phys. Lett. 67, (1979) 17

(7)   A. von Engel, "Ionized Gases", Oxford (1965)

(8)   P.F. Knewstubb and A.W. Tickner, J. Chem. Phys.
       36, (1962) 684; 37, (1962) 2941; 38, (1963) 464

(9)   F. Howorka, W. Lindinger and M. Pahl
       Int. J. Mass Spectrometry and Ion Physics 12, (1973) 67

(10)   D. Cossart, J. Chim. Phys. 76, (1979) 1045

(11)   D.D. Bičanič, Int. J. Infrared and Mm Waves 2, (1981) 247

(12)   F.C. van den Heuvel, W.L. Meerts, and A. Dymanus
       Chem. Phys. Lett. 88, (1982) 59

(13)   K.V.L.N. Sastry, P. Helminger, E. Herbst, and F.C. DeLucia
       Astrophys. J. 250 (1981) L91

(14)   K.V.L.N. Sastry, P. Helminger, E. Herbst, and F.C. DeLucia
       Chem. Phys. Lett. 84, (1981) 286

(15)   C.H. Townes and A.L. Schawlow, "Microwave Spectroscopy",
       McGraw-Hill, New York (1955)

(16)   R.C. Woods, T.A. Dixon, R.J. Saykally, and P.G. Szanto
       Phys. Rev. Lett. 35, (1975) 1269

Table 1   Observed rotational transitions

	lower J	$\nu_{obs.}$ a)	$\nu_{calc.}$ b)
HCO^+	8	802 459.7	802 459.3(0.5)
	10	980 637.4	980 638.6(0.8)
	11	1069 693.8	1069 696.6(1.0)
CO^+	15/2	1061 005.9	1061 005(3)
HN_2^+	10	1024 444.2	1024 445(6)

a. Frequencies given in MHz; experimental accuracy 1 MHz.

b. Calculation based on constants reproduced in Table 2.

Table 2   Molecular constants used for the calculation of transition
frequencies

	B_0 (MHz)	D_0 (kHz)	Ref.
HCO^+ $(X^1\Sigma)$	44 594.420(2)	82.39(7)	4
CO^+ $(X^2\Sigma)$ a)	58 983.040(12)	189.6(5)	13
HN_2^+ $(X^1\Sigma)$	46 586.863(15)	87.50(53)	14

a. Spin-rotation coupling constant γ_0 = 273.01(5) MHz
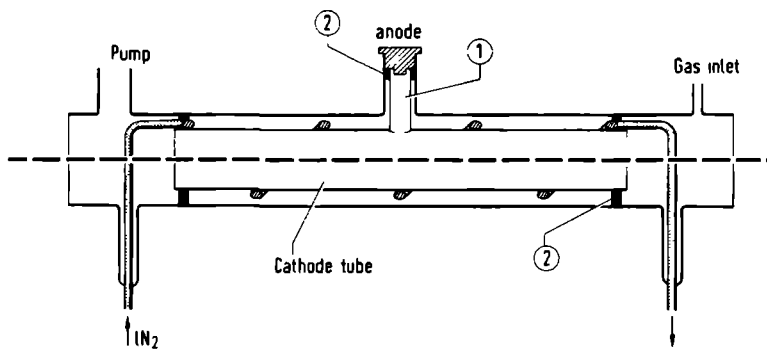
Fig. 1   Glass absorption cell with cold hollow cathode.

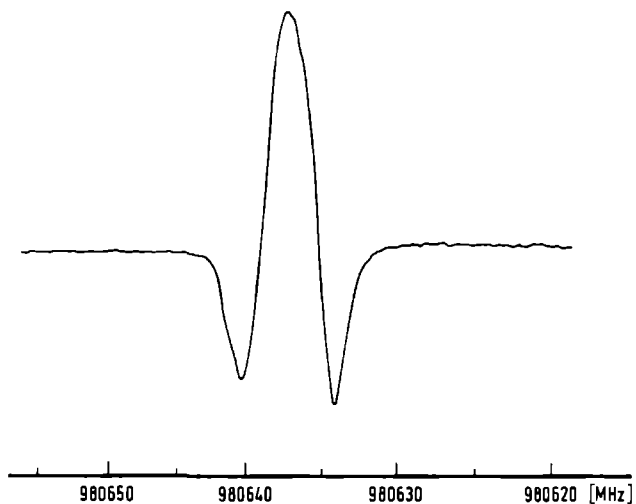1. Glass insert   2. Teflon seals

Fig. 2   The $J' = 11 \leftarrow J = 10$ rotational transition of HCO^+ ($v = 0$) observed using frequency modulation. Integration time 1 s, cell pressure 4 Pa, discharge current 300 mA.

3.5 The J=4 ← 3 rotational transition of DF at 2600 GHz.

Feasibility of high resolution spectroscopy with the laser-sideband spectrometer in the 3 THz (100 μm) range has been explored by observing the J=4 ← 3 rotational transition of deuterated hydrogen fluoride, DF $(X^1\Sigma(v=0))$. The experimental set-up was almost the same as for all spectroscopic studies described in the preceeding sections of this chapter, only the HCN laser was replaced by a water vapour laser, operating at 2528 GHz. The characteristics of this laser have been described in Sect.2.2.2. Also the antenna part of the mixer and the beam splitter foil of the diplexer were adjusted to operation at shorter wavelengths. The mixer turned out to produce tunable far-infrared radiation as efficiently as at frequencies around 1 THz (see Sect.2.5.4). No attempt was made to reduce absorption losses of radiation in the atmosphere outside the absorption cell.

The DF transition at 2600 GHz was detected in a natural sample of gaseous hydrogen fluoride. Despite very low (0.015%) abundance of this isotopic species, the line was easily observed. A frequency scan at relatively high cell pressure (25 Pa) is shown in Fig.13. In this scan the width of the line is slightly enlarged by pressure broadening.

The observed frequency is in good agreement with the value predicted from the molecular constants given by Sengupta *et al.* (SEN 79):

$\nu_{obs.}$ = 2600 176(2) MHz
$\nu_{calc.}$ = 2600 182(25) MHz

The accuracy of the observed value is determined by the manual setting of the laser frequency (cf. Sect.2.2), of the calculated one by limited accuracy of the constants.
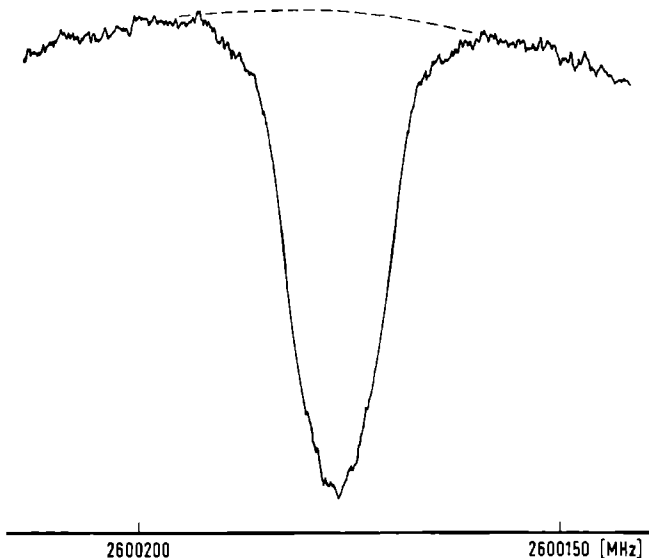
Figure 13 : Direct recording of the absorption due to the J=4←3 rotational transition of the DF molecule at 2.6 THz.

3.6 Unexpected molecular resonances

During spectroscopic investigations in DC glow discharges through various gas mixtures, a few molecular resonances have been observed accidentally. The resonances could be attributed neither to the molecule or ion that was searched for in the same spectral region, nor to the parent gases that were admitted to the cell. This is not surprising, since chemical reactions in a discharge are rather complex, yielding various reaction products. All lines mentioned below were observed in the water cooled discharge tube described in Sect.3.3.1. Absorption strength was at least 10% of TFIR power in all cases.

In search for the N=1 ← 0, J=2 ← 1 transition of the NH radical in a discharge through ammonia (Sect.3.3.5), an absorption line was observed which clearly could not be attributed to NH. Contrary to the lines of the paramagnetic

81

radical, the unexpected line could not be detected using Zeeman modulation. However, it was easily observable using on/off modulation (Sect.2.5.3). Absorption increased to 100% if pressure was reduced to about 1 Pa, which was far below optimal pressure for NH production (25 Pa). The molecule responsible for the mysterious line was stable. It was even produced by a continuous discharge or short current pulse through pure ammonia gas contained in a sealed-off absorption cell. Absorption intensity slowly diminished with time, after current was stopped in a sealed-off cell. The line was identified as the $J=11 \leftarrow 10$ rotational transition of the hydrogen cyanide (HCN) molecule, probably produced by reaction of ammonia discharge products with carbon atoms sputtered from the stainless steel cathode. The calculated and observed transition frequencies are given in Table 3.5. Calculation was based on

TABLE 3.5 : Unexpected molecular resonances

$\nu_{obs.}$ (MHz)	Discharged medium	Identification[a]		$\nu_{calc.}$ (MHz)
974 488.4(8)	NH_3 (+C)	HCN	10	974 487.2(4)
946 659(3)	CH_3OH	?	-	-
801 364(3)	H_2 + CO	H_2CO?	-	-
803 112(3)	H_2 + CO	H_2CO	$10_{3,7}$	803 111.6(2)
978 595(3)	H_2 + CO	H_2CO	$13_{1,13}$	978 592.5(3)
979 287(3)	H_2 + CO	H_2CO?	-	-

a) Quantum numbers correspond to the lower energy level involved in the transition; transitions are of the type $\Delta J=1$, and, in case of H_2CO, $\Delta K_{-1}=0$, $\Delta K_{+1}=1$.

standard formulas (TOW 55), and the molecular constants were taken from Winnewisser *et al.* (WIN 71). It should be noted that the coincidence of the NH and HCN lines is extremely fortuitous.

After observation of NH it turned out that the HCN line
appeared at a distance of only few MHz (about the linewidth)
from the closest hyperfine component of the NH rotational
transition, whereas the rotational lines of HCN are
separated by 88.6 GHz. A simultaneous recording of HCN and
NH is given in Fig.14. Discharge conditions were adjusted in
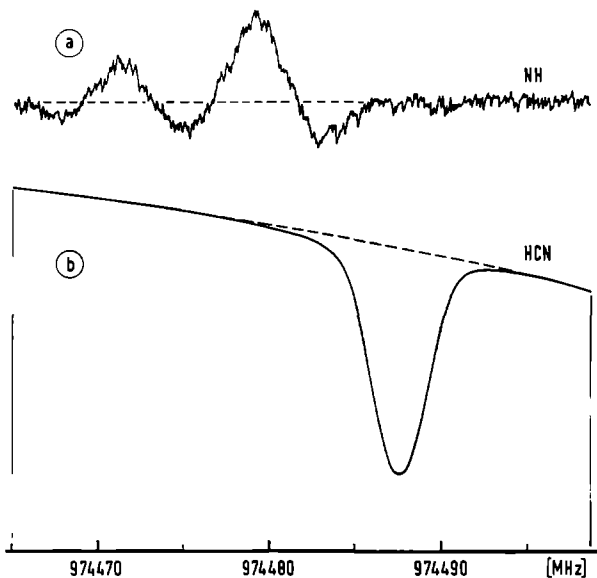
Figure 14 :   Simultaneous recording of resonances originating from the
              NH radical (upper trace) and the HCN molecule (lower trace),
              in a discharge through ammonia.
              Upper trace: lock-in no.1 tuned to Zeeman modulation; the HCN
                          line is invisible;
              Lower trace: lock-in no.2 tuned to on/off modulation; the NH
                          lines are invisible because of feeble absorption.
              Discharge conditions adjusted to favour the HCN line.

favour of the HCN line in this recording; Zeeman and on/off
modulation were applied simultaneously at two different
frequencies, with two lock-in amplifiers connected to the
bolometer.

A resonance of comparable intensity has been observed in a discharge through methanol (CH_3OH), at a frequency of 947 GHz (see Table 3.5). Again extremely strong absorption (95-100%) of TFIR power was observed, which could not be attributed to methanol itself. Optimal conditions were very much different from those for HCN. With a continuous discharge current through fast flowing methanol vapour, optimal pressure was about 20 Pa. In sharp contrast to behaviour in case of HCN, absorption intensity strongly increased with decreasing discharge current, with an optimum at the low value of 10 mA. In a sealed-off cell containing methanol, the unknown molecule was produced by a short pulse of current; absorption sustained afterwards. However, absorption disappeared within a fraction of a second if current was maintained. Attempts to identify the observed resonance did not lead to unambiguous results.

Finally, four resonances have been observed in a discharge through mixtures of hydrogen and carbon monoxide. This was the result of early searches for HCO^+. The molecule(s) responsible for the unexpected resonances was (were) produced both with flow and sealed-off operation of the cell. In both cases continuous discharge current proved to be essential. Two of the lines are identified as originating from the formaldehyde (H_2CO) molecule. Basis of this tentative conclusion is the near coincidence of the observed lines with those from a calculated spectrum of formaldehyde. The frequencies are compared in Table 3.5. The calculated frequencies given in this table were derived from the molecular constants determined by Cornet and Winnewisser (COR 80). The remaining two lines might originate from the same molecule and if so, will be associated with a vibrationally excited state. Support for this statement was obtained from a separate experiment. The line at 979.3 GHz, observed in the discharged H_2/CO mixture (Table 3.5), was recorded at the same frequency in a sample of almost pure formaldehyde, in absence of a discharge. In this case formaldehyde was produced by sublimation of paraformaldehyde outside the absorption cell. Absorption intensity was enhanced by a factor of two by striking a discharge through the sample.

High-Resolution Tunable Spectroscopy of Rotational Transitions of NO Near 30 cm⁻¹

F. C. van den Heuvel, W. Leo Meerts, and A. Dymanus

Fysisch Laboratorium, Katholieke Universiteit, Toernooiveld, Nijmegen 6525 ED, The Netherlands

The rotational spectrum of $^{14}N^{16}O$ is studied in the far infrared. The monochromatic tunable far-infrared radiation is generated by mixing the radiation of an HCN laser with that of a tunable klystron. Five rotational transitions in both the $^2\Pi_{1/2}$ and $^2\Pi_{3/2}$ states are observed in the frequency region between 852 and 1053 GHz. The results are compared with the known RF, microwave, and IR data.

1. INTRODUCTION

Recently it was shown (*1*, *2*) that it is possible to extend high-resolution spectroscopy towards the far infrared (FIR) by mixing the fixed frequency radiation of a submillimeter laser with that of a tunable klystron. The frequency of the generated radiation (laser sidebands) equals the sum or difference of the laser frequency and the klystron frequency. This radiation is tunable over the klystron range. We are now able to cover the spectral range from 780 to 1075 GHz (380–280 μm) using two lines (891 and 964 GHz) of an 8-m-long HCN laser and klystrons between 60 and 110 GHz. The absolute frequencies of five rotational transitions of NO in its ground vibrational electronic $^2\Pi$ state are determined with an accuracy of 3×10^{-7}. The resolution was Doppler limited to 2 MHz.

The lowest rotational transitions in the ground vibrational state of NO were studied in the past by several investigators (*3*, *4*, *5*). Recently an accurate study of the microwave spectrum below 500 GHz has been carried out by Pickett *et al.* (*6*). The far-infrared spectra obtained in the present investigation are compared with this spectrum and with radiofrequency Λ-doubling (*7*) and IR vibrational spectra (*8–11*). In order to do so we carried out an overall fit of all these data. The present FIR results are consistent with the already existing data on NO.

2. EXPERIMENTAL DETAILS

The experimental setup, shown in Fig. 1, is essentially that of Bicanic *et al.* (*1*). Radiation from the laser and a klystron is propagated through two separate arms of a modified crossed waveguide harmonic mixer to a Schottky barrier GaAs crystal–whisker assembly. Sidebands generated in the diode are reradiated by the whisker and leave the mixer through the third arm. Either the sum- or the difference-frequency sideband is selected and separated from fundamental laser radiation in a monochromator containing a reflection grating. Finally the selected sideband passes through a 2-m light pipe absorption cell filled with NO gas. Video detection
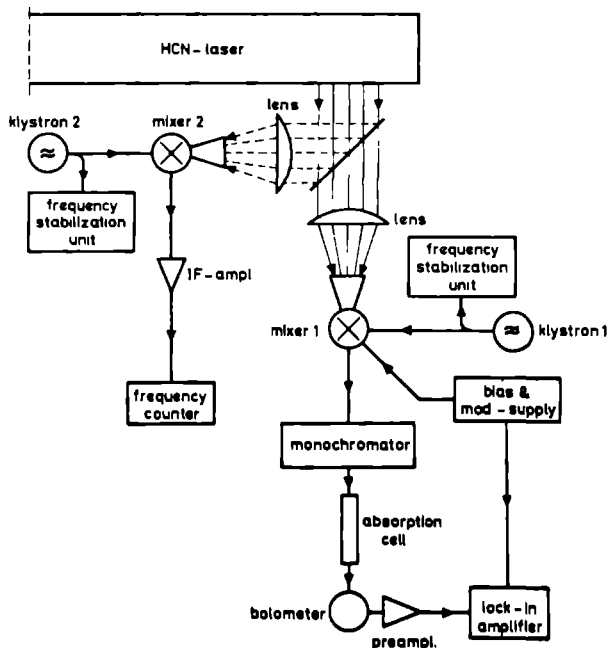
FIG. 1. Experimental setup with the sideband generator (mixer No. 1) and the laser frequency monitoring mixer (No. 2).

is applied with a helium-cooled bolometer. The sideband power at the input end of the monochromator is about 0.1–1 μW when a power of 50 and 150 mW enters the mixer from the laser and klystron, respectively. In an initial search for absorption lines the klystron was free-running and tuned mechanically and/or electrically. In precision measurements the klystron was phase-locked to a frequency standard.

Though the sidebands are highly monochromatic, there is an uncertainty in their absolute frequencies, because the free-running laser oscillates at an almost fixed but unknown frequency within its gain curve. This curve has a full width at half-height typically in the order of 2 and 3.5 MHz for the 964 and 891 GHz line, respectively. The uncertainty has been eliminated with the help of a second mixer that monitored the laser frequency during the measurements. A fraction of the laser beam traveling to the sideband generator is sent to this mixer, where the laser frequency beats with the 9th (891 GHz) or the 10th (964 GHz) harmonic of the frequency of a second phase-locked klystron operating at 99 or 96 GHz, respectively. A frequency counter monitors the amplified intermediate frequency (about 30 MHz) produced in the mixer. This technique has proven to be very effective for measuring the frequency of lasers in the entire far-infrared region (*12, 13*). The sideband frequency is known now with an accuracy of less than 50 kHz.

The transitions of NO were recorded with a signal-to-noise ratio of about 50 at a time constant of 1 sec and a cell pressure of 10 Pa. A typical recording is shown
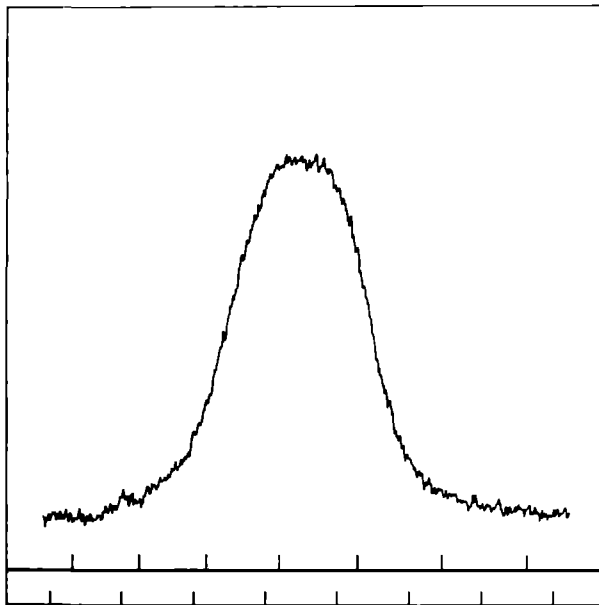
FIG 2 Typical recording of a rotational transition $^2\Pi_{1/2}$ $J = 19/2 \leftarrow 17/2$ of NO at 952 464 GHz Only one of the Λ components is shown $(+ \leftarrow -)$ The frequency of the scanning klystron is represented by the upper set of markers (spacing 2 MHz) the frequency of the laser by the lower set (spacing 0 01 MHz)

in Fig 2 The observed linewidths (FWHH) varied from 4 to 6 MHz, depending on the transition, and exceed the calculated Doppler widths (2–2 4 MHz) Broadening of the easily resolvable Λ-doubling components of the rotational transitions of NO is caused by the unresolved hyperfine structure Since the hyperfine splittings are known from molecular beam electric resonance (MBER) work (7, 14) and the relative intensities can easily be calculated, this information was used to fit the observed lineshape to the calculated one assuming the same Doppler width for each hyperfine component In Table I the frequencies of particular hyperfine line within each of the Λ-doubling components of a rotational transition are given

3 THEORY

The basic Hamiltonian for the spin–orbit, rotational and Λ-doubling contributions has been described in the classical papers of Hill (15) and Van Vleck (16) and of Mulliken and Christy (17) It has been shown in many investigations that an effective Hamiltonian for a $^2\Pi$ state can be constructed by applying a Van Vleck transformation to the $^2\Pi$, $^2\Sigma^s$ manifold of states in order to reduce the Hamilton matrix to two 2×2 $^2\Pi$ blocks each with different parity

As basis set we use the symmetrized Hund's case (a) wavefunctions (18) $\{|^2\Pi_{1/2}^{\pm}J\rangle, |^2\Pi_{3/2}^{\pm}J\rangle\}$ The effective Hamiltonian including the lowest-order cen-

TABLE I

Observed Rotational Transitions of $^{14}N^{16}O$ in Its Ground Vibrational and Electronic States

Ω	J+1 ← J	F+1 ← F	parity change	frequency [a]	obs.-calc. (MHz)	laser line (GHz)
		15/2 ← 13/2	+ ← -	851 913.54	0.40	964
1/2	17/2 ← 15/2					
		15/2 ← 13/2	- ← +	852 239.91	0.47	964
		17/2 ← 15/2	- ← +	952 145.08	-0.05	891
1/2	19/2 ← 17/2					
		17/2 ← 15/2	+ ← -	952 464.10	0.02	891
		21/2 ← 19/2	+ ← -	1052 369.91	0.23	964
1/2	21/2 ← 19/2					
		19/2 ← 17/2	- ← +	1052 680.83	0.10	964
		17/2 ← 15/2	+ ← -	875 930.36	0.00	964
3/2	17/2 ← 15/2					
		17/2 ← 15/2	- ← +	875 961.25	0.11	964
		19/2 ← 17/2	- ← +	978 770.21	-0.07	891
3/2	19/2 ← 17/2					
		19/2 ← 17/2	+ ← -	978 808.04	-0.24	891

[a] The experimental accuracy is 0.3 MHz, except for both $^2\Pi_{1/2}$, J = 17/2 ← 15/2 transitions (1 MHz).

trifugal distortion and spin–rotation effects (19) can be written as

$$(\mathscr{H}) = A \begin{bmatrix} -1/2 & 0 \\ 0 & 1/2 \end{bmatrix} + \frac{1}{2} A_D \begin{bmatrix} -(X+2) & 0 \\ 0 & (X-1) \end{bmatrix}$$

$$+ \gamma \begin{bmatrix} 0 & -(1/2)X^{1/2} \\ -(1/2)X^{1/2} & 0 \end{bmatrix} + B \begin{bmatrix} (X+1) & X^{1/2} \\ X^{1/2} & (X-1) \end{bmatrix}$$

$$- D \begin{bmatrix} (X+1)^2 + X & 2XX^{1/2} \\ 2XX^{1/2} & (X-1)^2 + X \end{bmatrix} \pm (-1)^{J-1/2}\left(J + \frac{1}{2}\right)\begin{bmatrix} ((1/2)p + q) & qX^{1/2} \\ qX^{1/2} & 0 \end{bmatrix}$$

$$+ \begin{bmatrix} (1/2)q^*(X+2) + (1/2)p^* + o & (1/2)(1/2p^* + q^*)X^{1/2} \\ (1/2)((1/2)p^* + q^*)X^{1/2} & (1/2)q^*X \end{bmatrix}, \quad (1)$$

where $X = (J + 1/2)^2 - 1$. The various contributions in this order stand for the spin–orbit (A), the centrifugal distortion in the spin–orbit coupling (A_D), the spin–rotation effect (γ), the rotational energy (B), the first-order centrifugal distortion effect on the rotational energy (D), the Λ-splittings contributions (p,q), and the parity-independent contributions (p^*,q^*,o) originating from the same interaction that produces the Λ-splitting. The constants A, A_D, γ, B, and D are defined as in the work of Zare *et al.* (19), while p, q, p^*, q^*, and o have been taken from the paper of Mulliken and Christy (17). As a consequence of the high correlations ($20, 21$) between the molecular constants from the Hamiltonian (1) an independent determination of all the molecular constants is not possible. Especially

A_D and γ are nearly totally correlated. The Hamiltonian (1) can be transformed into an effective Hamiltonian in which the correlations are removed

$$(\mathcal{H}) = A_{\text{eff}} \begin{bmatrix} -1/2 & 0 \\ 0 & 1/2 \end{bmatrix} + \frac{1}{2} A_{D_{\text{eff}}} \begin{bmatrix} -(X+2) & 0 \\ 0 & (X-1) \end{bmatrix}$$

$$+ B_{\text{eff}} \begin{bmatrix} (X+1) & X^{1/2} \\ X^{1/2} & (X-1) \end{bmatrix} - D \begin{bmatrix} (X+1)^2 + X & 2XX^{1/2} \\ 2XX^{1/2} & (X-1)^2 + X \end{bmatrix}$$

$$\pm (-1)^{J-1/2}(J + 1/2) \begin{bmatrix} ((1/2)p + q) & qX^{1/2} \\ qX^{1/2} & 0 \end{bmatrix} , \quad (2)$$

where

$$A_{\text{eff}} = A - \frac{1}{2} p^* - o,$$

$$A_{D_{\text{eff}}} = A_D - \frac{2B}{A - 2B} \left(\gamma - \frac{1}{2} p^* \right) ,$$

$$B_{\text{eff}} = B + \frac{1}{2} q^*. \qquad (3)$$

The relation for $A_{D_{\text{eff}}}$ is an approximation valid for $|A/B| \gg 1$. Higher-order centrifugal distortion effects are not relevant for the present study while higher-order Λ-doubling contributions can be treated in a phenomenological way (18, 22).

The choice of the effective Hamiltonian (2) is only one of the various possibilities that all lead to an equivalent power series expansion in the rotational quantum number J, however, with different effective parameters. Several of these possibilities have been used recently (9–11, 23, 24) in the analysis of the rotation–vibration spectrum of NO. The effective constants used in the present work are identical to those of Dale et al. (23), Henry et al. (9) and Hallin et al. (11). Both Amiot et al. (10) and Pine et al. (24) use slightly different definitions. Comparison

TABLE II

Effective Molecular Constants as Determined for NO in Various Investigations

	Present work [a]	Amiot et al. (10) [b]	Pine et al. (24) [c]
A_{eff}	$A - \frac{1}{2}p^* - o$	$A - \frac{1}{2}p^* - o - \frac{1}{2}p$	$A - \frac{1}{2}p^* - o - \frac{1}{2}p - [A_D - \frac{2B}{A-2B}(\gamma - \frac{1}{2}p^* - \frac{1}{2}p)]$
$A_{D\,\text{eff}}$	$A_D - \frac{2B}{A-2B}(\gamma - \frac{1}{2}p^*)$	$\frac{1}{2}[A_D - \frac{2B}{A-2B}(\gamma - \frac{1}{2}p^* - \frac{1}{2}p)]$	$A_D - \frac{2B}{A-2B}(\gamma - \frac{1}{2}p)$
B_{eff}	$B + \frac{1}{2}q^*$	$B + \frac{1}{2}q^* + \frac{1}{2}q$	$B + 2D + \frac{1}{2}q^* + \frac{1}{2}q$

[a] Same convention is used in ref. (9,11,23).

[b] Amiot et al. (10) use for $A_{D\,\text{eff}}$ the symbol $A_{J(\text{eff})}$.

[c] Pine et al. (24) have chosen to define the parameter o with an opposite sign.

of the results from the last two cited papers with those of the first group can be made with the help of Table II, where we express the effective constants in the basic molecular parameters from Eq. (1). Recently Young *et al.* (*25*) used a slightly different type of effective Hamiltonian. It is not possible to derive analytical relations similar to those of Table II between our effective constants and those of Young *et al.* since their energy expressions cannot be transformed to those of Eq. (2).

4 RESULTS

Recently two independent high-resolution IR spectroscopic studies of the (0–1) band were made by Amiot *et al.* (*10*) and Valentin *et al.* (*8*). We started with a fit of the data of Amiot *et al.* The microwave and FIR transitions predicted from this fit agree within the accuracy of the prediction with the observed line frequencies of the present work, of those of Refs. (*4, 5*), and of Pickett *et al.* (*6*). The latter authors recently performed very accurate measurements (0.02–0.05 MHz) of the rotational transitions $J = 5/2 \leftarrow 3/2, 7/2 \leftarrow 5/2$, and $9/2 \leftarrow 7/2$ for both the $^2\Pi_{1/2}$ and $^2\Pi_{3/2}$ substates and the $3/2 \leftarrow 1/2$ transitions for the $^2\Pi_{1/2}$ substate. If also these transitions are included in a combined fit with the data of Amiot *et al.* the constants obtained by Amiot *et al.* do not change but only the accuracy of many of them is improved.

We repeated the fit procedure starting with the data of Valentin *et al.* The microwave and far-infrared transitions predicted only from a fit of the IR data deviated from the experimental microwave and FIR frequencies outside the accuracy of the prediction. Furthermore, the best fit constants changed to values outside their error limits in a combined fit of Valentin's IR, all the available microwave data, and the results of the present investigation. In conclusion we feel that the data of Amiot *et al.* provide a slightly better overall consistency with the microwave and FIR spectra.

In a final least-squares fit we combined the 347 (0–1) IR transitions (Amiot *et al.*), the FIR transitions from the present work and the microwave transitions from Refs. (*4–6*) with the hyperfine Λ-doubling transitions from an MBER study (*7, 14*). The latter transitions determine mainly the Λ-doubling parameters p and q, as well as the hyperfine structure which we do not discuss here. The results of the calculations are presented in Table III. The overall fit is excellent. The combination of the MBER, microwave, FIR, and IR data improves considerably the accuracy of the rotational and the Λ-doubling constants. It should be noted here that the uncertainties in the constants B_{eff}, D, and $A_{D_{\text{eff}}}$ for the ground vibrational state are mainly determined by the microwave data of Pickett *et al.* (*6*). The differences between the predicted spectrum for the best fit constants and the present experimental frequencies are listed in Table I, demonstrating an excellent consistency between the present FIR and the microwave data of Ref. (*6*).

We have also tried to include the second-order centrifugal distortion effects described by the constant H (see, e.g., (*19*)). This gave no significant improvement of the fit, while only an upper limit ($|H| < 2 \times 10^{-2}$ Hz) for H could be obtained.

TABLE III

Best-Fit Constants from a Fit of the IR Data (10) only, and of the IR, Microwave, FIR, and MBER Data

Quantity [a]	IR-data [b]	IR+MW+MBER-data [c]
$A_{eff\ 0}$	3 691.626(5)	3 691.619(3)
$A_{D\ eff\ 0}$	5.46(2)	5.496(2)
$B_{eff\ 0}$	50 847.7(1)	50 847.801(1)
D_0	0.1641(2)	0.16416(3)
p_0	350.8(3)	350.3750(2)
q_0	2.82(2)	2.8373(1)
$A_{eff\ 1}$	3 684.295(5)	3 684.290(4)
$A_{D\ eff\ 1}$	5.20(2)	5.230(8)
$B_{eff\ 1}$	50 321.0(1)*	50 321.03(1)
D_1	0.1646(2)	0.16463(3)
p_1	348.9(3)	348.6(2)
q_1	2.81(2)	2.827(8)
No. lines	347	482
σ [d]	0.63	0.75

[a] All constants are in units of MHz, except A, which is given in GHz.

[b] After the transformation given in Table II the set of constants becomes the same as obtained by Amiot et al. (10).

[c] IR ref. (10), FIR (present work), microwave ref. ($4,5,6$), MBER ref. ($7,14$). The centrifugal distortion corrections in p_0 and q_0 were also taken into account (18): $D_{p_0} = 91(2)$ Hz and $D_{q_0} = 21(2)$ Hz.

[d] $\sigma = \sqrt{\chi^2/(n-m)}$, n number of lines, m number of parameters determined in the fit.

We conclude that the technique of sideband generation in combination with a continuous monitoring of the laser frequency is well suited for Doppler-limited high-resolution spectroscopy around 30 cm^{-1}.

REFERENCES

1 D D BICANIC, B F J ZUIDBERG, AND A DYMANUS, *Appl Phys Lett* **32**, 367–369 (1978)

2 D D BICANIC, Ph D thesis, Katholieke Universiteit, Nijmegen, The Netherlands, 1978

3 J J GALLAGHER AND C M JOHNSON, *Phys Rev* **103**, 1727–1737 (1956)

4 C A BURRUS AND J D GRAYBEAL, *Phys Rev* **109**, 1553–1556 (1958)

5 P G FAVERO, A M MIRRI, AND W GORDY, *Phys Rev* **114**, 1534–1537 (1959)

6 H M PICKETT, E A COHEN, J W WATERS, AND T G PHILLIPS, 34th Symposium on Molecular Spectroscopy, Columbus, Ohio (1979) private communication

7 W L MEERTS AND A DYMANUS, *J Mol Spectrosc* **44**, 320–346 (1972)

8 A VALENTIN, A HENRY, PH CARDINET, M F LEMOAL, DA-WUN CHEN, AND K NARAHARI RAO, *J Mol Spectrosc* **70**, 9–17 (1978)

9 A HENRY, M F LEMOAL, PH CARDINET, A VALENTIN, *J Mol Spectrosc* **70**, 18–26 (1978)

10 C AMIOT, R BACIS, AND G GUELACHVILI, *Canad J Phys* **56**, 251–265 (1978)

11 K-E HALLIN, J W C JOHNS, D W LEPARD, A W MANTZ, D L WALL, AND K NARAHARI RAO, *J Mol Spectrosc* **74**, 26–42 (1979)

12 B F J ZUIDBERG AND A DYMANUS, *Appl Phys Lett* **29**, 643–645 (1976)

13 V J CORCORAN, J J GALLAGHER, AND R E CUPP, *Opt Spectra* **4**, 46–51 (1970)

14 W L MEERTS, *Chem Phys* **14**, 421–425 (1976)

15 E HILL, J H VAN VLECK, *Phys Rev* **32**, 250–272 (1928)

16 J H VAN VLECK *Phys Rev* **33**, 467–506 (1929)

17 R S MULLIKEN AND A CHRISTY, *Phys Rev* **38**, 87–119 (1931)

18 W L MEERTS, J P BEKOOY AND A DYMANUS, *Mol Phys* **37**, 425–439 (1979)

19 R N ZARE, A L SCHMELTEKOPF, W J HARROP, AND D L ALBRITTON, *J Mol Spectrosc* **46**, 37–66 (1973)

20 J A COXON, *J Mol Spectrosc* **58**, 1–28 (1975)

21 D L ALBRITTON, W J HARROP, A L SCHMELTEKOPF, R N ZARE, AND E L CROW, *J Mol Spectrosc* **46**, 67–88 (1973)

22 W L MEERTS, *Chem Phys Lett* **46**, 24–28 (1977)

23 R M DALE, J W C JOHNS, A R W MCKELLAR, M RIGGIN, *J Mol Spectrosc* **67**, 440–458 (1977)

24 A S PINE, J W C JOHNS, AND A G ROBIETTE, *J Mol Spectrosc* **74**, 52–69 (1979)

25 L D G YOUNG, A T YOUNG, S A CLOUGH, AND F X KNEIZYS, *J Quant Radiat Transfer* **20**, 317–325 (1978)

THE FAR-INFRARED ROTATIONAL SPECTRUM OF THE CF RADICAL

F C VAN DEN HEUVEL, W Leo MEERTS and A DYMANUS

Fysisch Laboratorium, Katholieke Universiteit Nijmegen, 6525 ED Nijmegen, The Netherlands

The rotational spectrum of CF in its ground electronic state was studied around 1000 GHz using a tunable far infrared source Seven transitions were observed originating from the $^2\Pi_{1/2}$ and $^2\Pi_{3/2}$ substates The hyperfine and Λ-type split tings were resolved The results were combined with gas phase electron resonance and infrared diode laser spectra to determine all pertinent molecular constants

1 Introduction

The spectrum of the CF radical has been studied in the past by electronic [1,2] and infrared diode laser spectroscopy [3], by gas-phase electron-paramagnetic (EPR) [4], and laser magnetic resonance (LMR) [5], and by microwave spectroscopy [6] However, since the Λ-doubling parameter q was still undetermined and of the magnetic hyperfine constants only a linear combination was known [4], it was felt necessary to investigate in more detail the rotational spectra of CF in the ground vibronic state Several rotational transitions $J + 1 \leftarrow J$ for J ranging from 17/2 to 23/2 in both the $^2\Pi_{1/2}$ and $^2\Pi_{3/2}$ sublevels fall within the range of our FIR side-band spectrometer These spectra have been studied with high resolution in zero magnetic field Both the Λ-doubling and hyperfine structure was resolved Besides the normal rotational constants B and D, we determined the two Λ-doubling constants p and q and the four magnetic hyperfine parameters a, b, c and d of Frosh and Foley

2. Experiment and results

The FIR side-band spectrometer has been described in detail elsewhere [7,8] The radiation of a fixed-frequency HCN laser and that of a tunable millimeter wave klystron were mixed on a diode The diode generated two beams of tunable far infrared

radiation with a frequency equal to the sum and difference of the fundamental frequencies of laser and klystron (laser side-bands) The diode which was of the Schottky barrier type was mounted in a mixer with semi-open structure, i e the microwave radiation was transmitted to the diode via a normal closed rectangular waveguide penetrated by the diode stud, whereas far-infrared radiation was transported towards and from the diode via a whisker antenna mounted in free space A Michelson-type interferometer [9] separated the side-bands from fundamental laser radiation and a simple monochromator was used to select the side-band beam corresponding to either the sum or difference frequency The tunable side-band radiation then passed through a 1 m long absorption cell and was detected by a helium-cooled bolometer

For each required side band frequency the HCN laser was free running at one of its strongest lines at 890 7603 and 964 3127 GHz [8] During the measurements the laser was set manually at the top of the gain profile It was found that by this procedure the accuracy of the laser frequency setting was ±0 8 MHz

The CF radicals were produced by a dc glow discharge in a gas mixture rapidly flowing through the absorption cell Several combinations of gases have been investigated The best signals were obtained with a mixture of either argon and CF_4 or argon, CF_4 and methyl fluoride The total pressure was in the region below 75 mbar and the discharge current be-

Table 1
Observed and calculated rotational transition $(J + 1, F) \leftarrow (J, F')$ (in MHz) of CF in its ground vibrational state

Ω	$J + 1$	F [a]	F'	Label	Observed frequency	Obs. − calc.
1/2	19/2	9e	8e	ν_1	786 742.7(8)	−0.3
		10e	9e	ν_2	786 745.8(8)	−0.6
		10f	9f	ν_3	786 974.1(8) [b]	−
		9f	8f	ν_4	786 976.6(8)	0.3
				$\nu_3 - \nu_2$	228.3(8)	−0.2
1/2	21/2	10e	9e	ν_5	869 612.7(8)	0.5
		11e	10e	ν_6	869 616.7(8) [b]	−
		10f	9f }	ν_7	869 840.0(8) [b]	−
		11f	10f			
				$\nu_6 - \nu_5$	4.0(4)	0.1
				$\nu_7 - \nu_5$	223.3(8)	0.2
1/2	23/2	11e	10e	ν_8	952 484.6(8)	0.7
		12e	11e	ν_9	952 488.7(8) [b]	−
		11f	10f }	ν_{10}	952 705.8(8) [b]	−
		12f	11f			
				$\nu_9 - \nu_8$	4.1(4)	−0.2
				$\nu_{10} - \nu_8$	217.1(8)	−0.1
1/2	25/2	12e	11e	ν_{11}	1035 354.2(8)	0.4
		13e	12e	ν_{12}	1035 359.0(8) [b]	−
		12f	11f }	ν_{13}	1035 569.9(8) [b]	−
		13f	12f			
				$\nu_{12} - \nu_{11}$	4.8(3)	0.3
				$\nu_{13} - \nu_{11}$	210.9(8)	−0.2
3/2	19/2	10e	9e	ν_{14}	815 230.5(8)	−0.0
		9e	8e	ν_{15}	815 248.4(8) [b]	−
		10f	9f	ν_{16}	815 261.0(8) [b]	−
		9f	8f	ν_{17}	815 274.3(8) [b]	−
				$\nu_{15} - \nu_{14}$	17.9(2)	0.2
				$\nu_{16} - \nu_{15}$	12.7(2)	−0.2
				$\nu_{17} - \nu_{16}$	13.3(2)	−0.0
3/2	21/2	11e	10e	ν_{18}	900 671.8(8)	0.1
		10e	9e	ν_{19}	900 687.3(8) [b]	−
		11f	10f	ν_{20}	900 708.2(8) [b]	−
		10f	9f	ν_{21}	900 719.1(8) [b]	−
				$\nu_{19} - \nu_{18}$	15.5(2)	−0.1
				$\nu_{20} - \nu_{19}$	20.9(8)	0.4
				$\nu_{21} - \nu_{20}$	10.9(2)	−0.0
3/2	25/2	13e	12e	ν_{22}	1071 239.7(8)	−0.1
		12e	11e	ν_{23}	1071 252.2(8) [b]	−
		13f	12f	ν_{24}	1071 287.9(8) [b]	−
		12f	11f	ν_{25}	1071 294.9(8) [b]	−
				$\nu_{23} - \nu_{22}$	12.6(6)	−0.2
				$\nu_{24} - \nu_{23}$	35.0(3)	0.2
				$\nu_{25} - \nu_{24}$	7.7(3)	0.1

[a] The e/f convention for labeling the levels suggested by Brown et al. [10] has been followed.
[b] This line was left out of the fit; as indicated below, the difference of this line with another of the same rotational transition has been included.

tween 50 and 200 mA. Under these conditions it was possible to observe spectra of CF for several hours before cleaning of the cell became necessary.

To facilitate phase-sensitive detection Zeeman modulation has been applied. The modulation field was generated by a coil wrapped around the absorption cell, which produced a sine wave magnetic field alternating between 0 and ≈ 7.5 mT. The signal-to-noise ratio under optimum conditions varied between 10 and 50 at an integration time of 1 s. The full linewidth of the observed absorption lines was 2–3 MHz which is the Doppler limit at these frequencies. A list of the observed transition frequencies is given in table 1. The $\Pi_{3/2}$, $J = 23/2 \leftarrow 21/2$ transition is missing from this list, because it was unobservable due to strong absorption by atmospheric water vapour at 986 GHz. The accuracy in the absolute frequency of each line was limited by the uncertainty to which the HCN laser frequency could be set (0.8 MHz). The drift in the frequency of the free running laser was negligible during the short time interval of measurement of a single rotational transition. Consequently small splittings between the hyperfine Λ-doubling components of a rotational transition could be measured more accurately. The uncertainties in the splittings were dominated by the accuracy to which the peak frequencies of the individual components could be determined. Table 1 also lists these splittings.

3. Analysis and discussion

In order to obtain an accurate and as complete as possible set of the molecular parameters of CF we combined the present FIR spectra with most of the data available in the literature. The hamiltonian discussed in ref. [8] provides an adequate description of the fine structure contributions to the energy of a molecule in a $^2\Pi$ electronic state [‡]. This hamiltonian is based on a power-series expansion in R^2, where R is the angular momentum of the nuclei. However, it was shown [11] on theoretical grounds that a hamiltonian expanded as a power series in N^2 is to be

[‡] Eqs. (1) and (2) of the hamiltonian presented in ref. [8] contain two unfortunate misprints. In both equations the diagonal element for $\Omega = 1/2$ of A_D should read $-(X + 1)$, while the off-diagonal matrix element of the parity dependent Λ-doubling should read $\frac{1}{2}qX^{1/2}$.

Table 2
The molecular constants of CF($X\,^2\Pi$) in the $\upsilon = 0$ and $\upsilon = 1$ vibrational states. All values are in MHz, except A_{eff} and ν_0, which are in cm^{-1}

	$\upsilon = 0$	$\upsilon = 1$
A_{eff} [a]	77.11(1)	76.46(1)
$A_{D,eff}$	−7.94(22)	−7.98(30)
B_{eff}	42197.031(59)	41651.42(17)
D	0.19870(23)	0.19629(56)
P	255.60(35)	253.6(1.5)
q	0.760(14)	
a	633(29)	
b	261(6)	
$b + \frac{1}{3}c$	195(18)	
d	772(27)	
c(calc)	−200(61)	
h(calc.) [a]	663.5(3.0)	
ν_0		1286.14639(24)

[a] $A_{eff}(\upsilon = 0)$ and h were restrained to 77.11(1) cm^{-1} [1] and 662.9(30) MHz [4], respectively (see text).

preferred; here $N = R + L$, with L being the electronic orbital momentum. We decided to follow this recommendation and the resulting molecular constants for CF given in table 2 are from a fit to the N^2-type hamiltonian. Explicit expressions for matrix elements of the N^2-type hamiltonian were recently published by Amiot et al. (ref. [12], table 2). The expansion in powers of the quantum number J of the total angular momentum is only slightly different for the R^2- and N^2-type hamiltonian and the only two major changes involve the rotational constant B and the vibrational energy spacing ν_0:

$$B_{eff,\upsilon}(N^2) - B_{eff,\upsilon}(R^2) = 2D_\upsilon , \tag{1}$$

$$\nu_0(N^2) - \nu_0(R^2) = B_{eff,1}(N^2) - B_{eff,0}(N^2). \tag{2}$$

The hyperfine structure in CF can properly be described by the four parameters a, b, c and d of Frosh and Foley (for matrix elements see e.g. ref. [13]).

Recently Kawaguchi et al. [3] analyzed their diode laser spectra of the $\upsilon = 0 \rightarrow 1$ vibrational transition in CF using the R^2-type hamiltonian. The parameter A_J^{eff} they use to describe the centrifugal distortion effect in the spin–orbit differs slightly from our $A_{D,eff}$. It can easily be shown that

$$A_{D,eff} = 2A_J^{eff} + Bp/(A - 2B) . \tag{3}$$

As a check we reanalysed the data of Kawaguchi et al.

and found perfect agreement taking into account the relations (1)–(3) In the next step we added the present FIR data from table 2 For each rotational transition (except $\Pi_{1/2}, J = 19/2 \leftarrow 17/2$) we included in the fit the absolute frequency of one of the hyperfine Λ doubling components and the frequency distances of the others, as indicated in table 1 In the cases of unresolved transitions the calculated average of these transitions was fitted to the observed frequency This allowed us to reduce the uncertainty in some of the fine structure constants, and in addition to determine the Λ-doubling constant q and all the hyperfine structure parameters

Two further steps were undertaken to improve the accuracy of the parameters of CF Since the correlation between $A_{eff,0}$ and $A_{eff,1}$ has been removed in the combined set of FIR and IR data both parameters could be obtained The results were in excellent agreement with those of Porter et al [1] However, the accuracy for $A_{eff,0}$ of Porter et al was still about a factor of five higher We therefore restricted $A_{eff,0}$ to the value 77 11(1) cm^{-1} of Porter et al and allowed this constant to vary within the given accuracy

A similar situation occurred with the hyperfine parameters The present FIR data allow an independent determination of all four hyperfine parameters Carrington and Howard [4] obtained from their EPR studies of CF $b = 190(50)$ MHz and a linear combination between a, b and c

$$h = a + \tfrac{1}{2}(b + c) = 662\ 9(3\ 0)\ \text{MHz} \qquad (4)$$

The value for h we derived purely from the FIR spectra was in agreement with that of Carrington and Howard However, their uncertainty in this constant was about a factor of 10 smaller than ours We therefore restrained h to 662 9(3 0) MHz, again free to vary within its error limits This procedure considerably improved the accuracy of the four independent hyperfine structure parameters The constants obtained from the final least squares fit are in table 2 The agreement between the results of the best fit calculation and the experimental frequencies is excellent as can be seen from table 2

Since all four hyperfine structure parameters for the ground vibrational state are now known, an independent determination of the expectation values associated with the unpaired electron is made possible Using relations given before [14] we find $\langle 1/r^3 \rangle_U = 8\ 50(40)$, $\langle (3\cos^2\theta - 1)/r^3 \rangle_U = -1\ 78(57)$,

$\langle \sin^2\theta/r^3 \rangle_U = 6\ 94(24)$ and $\langle \Psi^2(0) \rangle_U = 0\ 313(29)$, all in units of 10^{24} cm^{-3} It follows that the ratios between the first three quantities is not equal to that of a pure p orbital centered at the fluorine atom $(4/5) \quad (-2/5) \quad 1$ It also follows that the assumption of Carrington and Howard [4] that the contribution to the Fermi contact term $\langle \Psi^2(0) \rangle_U$ arises mainly from the fluorine s atomic orbital is too simple

The prediction from SCF calculations by Hall and Richards [15] is $\langle 1/r^3 \rangle = 8\ 5$ and $\langle (3\cos^2\theta - 1)/r^3 \rangle = -2\ 9$, in units of 10^{24} cm^{-3} Although the authors claim that their method of calculation predicts the spin distributions poorly, their results are in quite good agreement with the present experimental values

Acknowledgement

References

[1] T L Porter, D E Mann and N Aquista, J Mol Spectry 16 (1965) 228
[2] D K Carroll and T P Grennan, J Phys B3 (1970) 865
[3] K Kawaguchi, C Yamada, Y Hamada and E Hirota, J Mol Spectry 86 (1981) 136
[4] A Carrington and B J Howard, Mol Phys 18 (1970) 225
[5] R J Saykally and K M Evenson, 34th Symposium on Molecular Spectroscopy, Columbus, Ohio, 1979, paper TF4
[6] S Saito, Y Endo and E Hirota, 41st Annual Meeting of the Chemical Society of Japan Osaka, 1980, paper 1D31
[7] D D Bicanic, Intern J Infrared Millimeter Waves 2 (1981) 247
[8] F C van den Heuvel, W L Meerts and A Dymanus, J Mol Spectry 84 (1980) 162
[9] N R Erickson, IEEE Trans. MTT 25 (1977) 865
[10] J M Brown J T Hougan K P Huber, J W C Johns, I Kopp, H Lefebvre Brion, A J Merer, D A Ramsay, J Rostas and R N Zare, J Mol Spectry 55 (1975) 500
[11] J M Brown, E A Colbourn, J K G Watson and F D Wayne, J Mol Spectry 74 (1979) 294
[12] C Amiot, J -P Maillard and J Chauville, J Mol Spectry 87 (1981) 196
[13] W L Meerts, J P Bekooy and A Dymanus, Mol Phys 37 (1979) 425
[14] W L Meerts and A Dymanus, Can J Phys 53 (1975) 2123
[15] J A Hall and W G Richards, Mol Phys. 23 (1972) 331

The laser-sideband spectrometer has been applied successfully
to high resolution spectroscopic studies in the far-infrared.
It would be rather exceptional in experimental physics if the
design of the spectrometer was not susceptible to further im-
provements. Indeed it should be possible to increase sensiti-
vity by pushing the mixer to still higher production of tunable
far-infrared radiation. In the near future, semiconductor
technology might provide diode chips especially designed for
present application. The diode chips used up till now were
designed especially for use in heterodyne detectors of micro-
wave radiation and not for generation of laser-sideband
radiation at THz frequencies. Transmission of microwave power
to the diode is more efficient via the whisker than via the
diode stud. A change of the mixer design in this sense will not
lead to higher TFIR power, because of saturation and burn-out
effects. However, such a change will lower the required power
level and clear the way to introduction of less powerful micro-
wave sources, with more favourable characteristics for present
application than klystrons. Extension to a complete coverage of
the far-infrared (1-4 THz) is a logical step after the
pioneering experiments at 2.6 THz. Optically pumped molecular
lasers should be used instead of the few powerful discharge
lasers existing in this region. Then, it is worthwhile to
replace the klystrons as sources of microwave radiation by
backward-wave oscillators. The larger tuning range and smooth
tunability of these devices will improve flexibility of the
experimental set-up, when searching for lines of little-known
compounds or molecular fragments.

Chapter 3 gives an impression of the capabilities of the
laser-sideband spectrometer. Molecules with internal motion
have been studied in the excited vibrational state and spectra
of light radicals and ions have been recorded and analyzed.
Obviously there are various possibilities for continuation of
the line of investigation. Most promising is the topic of

radical and ion spectroscopy. In astrophysics there is great interest for detailed spectroscopic information about these species. Spectra observed from interstellar space and stellar atmospheres can be identified with the aid of laboratory results. In this way the combination of laboratory experiments and astronomical observations leads to better insight in the abundance of various chemical compounds and reaction chemistry in space.The effective sensitivity and resolution of the present far-infrared spectrometer is comparable to that of microwave spectrometers. However, the latter ones cannot be used to study light compounds, especially those of astro-physical importance, composed of H, C, Si, N, O and S atoms. In view of sensitivity required for ion spectroscopy, it is advisable to apply the sideband spectrometer for investigation of species with a relatively large electric dipole moment. This choice gives some reserve in case the experimental efficiency of ion production does not come up to (usually rough) estimates.

ALI 76   M.R.Aliev,and J.K.G.Watson,J.Mol.Spectrosc.61 (1976) 29

AMI 79   C.Amiot,and G.Guelachvili,J.Mol.Spectrosc.76 (1979) 86

BEL 80   S.P.Belov,L.I.Gershtein,A.F.Krupnov,A.V.Maslovskij,S.Urban,
          V.Spirko,and D.Papousek,J.Mol.Spectrosc.84 (1980) 288

BIC 78   D.D.Bićanić,Ph.D.Thesis,Katholieke Universiteit Nijmegen (1978)

BIC 78a   D.D.Bićanić,B.F.J.Zuidberg,and A.Dymanus,Appl.Phys.Lett.32 (1978)
          367

BIC 81   D.D.Bićanić,Int.J.Infrared and Mm Waves 2 (1981) 247

BLU 79   W.A.M.Blumberg,H.R.Fetterman,D.D.Peck,and P.F.Goldsmith,Appl.Phys.
          Lett.35 (1979) 582

BLU 81   W.A.M.Blumberg,D.D.Peck,and H.R.Fetterman,Appl.Phys.Lett.39 (1981)
          857

BRA 72   C.C.Bradley,Infrared Phys.12 (1972) 287

BRO 82   J.M.Brown,and J.E.Schubert,J.Mol.Spectrosc. (1982),to be published

CAR 67   A.Carrington,D.H.Levy,and T.A.Miller,Mol.Phys.13 (1967) 401

CAR 69   C.Carlone,and F.W.Dalby,Can.J.Phys.47 (1969) 1945

CLA 81   P.F.Clancy, '6th Int.Conf.on Infrared and Mm Waves',Miami Beach,
          Florida USA (1981)

CLI 71   B.J.Clifton,W.T.Lindley,R.W.Chick,and R.A.Cohen, 'Proc.3rd
          biennial Cornell electrical engineering conference',Itaca,New
          York (1971)

CLY 73   M.A.A.Clyne,J.A.Coxon,and A.R.Woon Pat,J.Mol.Spectrosc.46 (1973)
          146

COR 80   R.Cornet,and G.Winnewisser,J.Mol.Spectrosc.80 (1980) 438

DIJ 71   F.A.van Dijk,Ph.D.thesis,Katholieke Universiteit Nijmegen (1971)

DOU 55   G.C.Dousmanis,T.M.Sanders,and C.H.Townes,Phys.Rev.100 (1955) 1735

EDM 57   A.R.Edmonds, 'Angular momentum in quantum mechanics',Princeton
          University Press,New Jersey (1957)

ERI 77   N.R.Erickson,IEEE Tr.MTT-25 (1977) 865

FET 78   H.R.Fetterman,P.E.Tannenwald,B.J.Clifton,C.D.Parker,W.D.Fitzgerald,
          and N.R.Erickson,Appl.Phys.Lett.33 (1978) 151

FRE 67   L.Frenkel,T.Sullivan,M.A.Pollack,and T.J.Bridges,Appl.Phys.Lett. **11** (1967) 344

FRE 70   R.S.Freund,T.A.Miller,D.de Santis,and A.Lurio,J.Chem.Phys.**53** (1970) 2290

FRE 76   S.M.Freund,and T.Oka,Phys.Rev.**A13** (1976) 2178

FRO 52   R.A.Frosch,and H.M.Foley,Phys.Rev.**88** (1952) 1337

GAL 56   J.J.Gallagher,and C.M.Johnson,Phys.Rev.**103** (1956) 1727

GOR 70   W.Gordy,and R.L.Cook, 'Microwave Molecular Spectra',Interscience, New York (1970)

HEN 57   J.M.Henrie,and P.Kusch , Phys.Rev.**107** (1957) 716

HEU 80   F.C.van den Heuvel,W.L.Meerts,and A.Dymanus,J.Mol.Spectrosc.**84** (1980) 162;paper no.1 in this thesis

HEU 82   F.C.van den Heuvel,W.L.Meerts,and A.Dymanus,Chem.Phys.Lett.**88** (1982) 59;paper no.2 in this thesis

HUY 79   M.J.Huyben,C.G.C.M.de Kort,J.H.M.Stoelinga,and P.Wyder,Infrared Phys.**19** (1979) 257

JAS 61   H.Jasik, 'Antenna Engineering Handbook',McGraw-Hill,New York (1961)

JON 78   H.Jones,Appl.Phys.**15** (1978) 261

JUD 63   B.R.Judd, 'Operator techniques in atomic spectroscopy',McGraw-Hill,New York (1963)

KRA 77   H.Kräutle,E.Sauter,and G.V.Schultz,Infrared Phys.**17** (1977) 477

KRA 78   H.Kräutle,E.Sauter,and G.V.Schultz, 'Proc.3rd internat.conference on submillimeter waves and their applications',Guildford,U.K. 1978;Infrared Phys.**18** (1978) 705

MAR 78   A.de Martino,R.Frey,and F.Pradere,Opt.Comm.**27** (1978) 262

MEE 72   W.L.Meerts,and A.Dymanus,J.Mol.Spectrosc.**44** (1972) 320

MEE 73   W.L.Meerts,and A.Dymanus,Astrophys.J.**180** (1973) L93

MEE 78   W.L.Meerts,and I.Ozier,Phys.Rev.Lett.**41** (1978) 1109

MEE 82a   W.L.Meerts,and I.Ozier,to be published (1982)

MEE 82b   W.L.Meerts,and I.Ozier,private communication (1982)

MEU 76   J.J.ter Meulen,Ph.D.Thesis,Katholieke Universiteit Nijmegen (1976)

NIE 47   H.H.Nielsen,and D.M.Dennisson,Phys.Rev.**72** (1947) 86L;1101

PAR 78   N.Paraire,S.Laval,and R.Laval,Infrared Phys.**18** (1978) 545

PIC 81   H.M.Pickett,E.A.Cohen,D.E.Brinza,and M.M.Schaefer,J.Mol.Spectrosc.
          89 (1981) 542

POY 75   R.L.Poynter,and R.K.Kakar,Astrophys.J.Suppl.29 (1975) 87

RAD 81   H.E.Radford,K.M.Evenson,and D.A.Jennings,Chem.Phys.Lett.78 (1981)
          589

ROS 81   H.P.Röser,G.V.Schultz,and R.Wattenbach, '6th Int.Conf.on Infrared
          and Mm Waves',Miami Beach,Florida USA (1981)

SAK 78   K.Sakai,K.Ichimura,H.Masumoto,and Y.Kitagawa,Infrared Phys.18
          (1978) 577

SAY 79   R.J.Saykally,and K.M.Evenson,Phys.Rev.Lett.43 (1979) 515

SEN 79   U.K.Sengupta,P.K.Das,and K.Narahari Rao,J.Mol.Spectrosc.74 (1979)
          322

SHI 69   F.Shimizu,J.Chem.Phys.52 (1969) 3572

TOW 55   C.H.Townes,and A.L.Schawlow, 'Microwave Spectroscopy',McGraw-Hill,
          New York (1955)

ULR 78   B.T.Ulrich,Infrared Phys.18 (1978) 429

URB 80   S.Urban,V.Spirko,D.Papousek,R.S.McDowell,N.G.Nereson,S.P.Below,L.I.
          Gershtein,A.V.Maslovskij,A.F.Krupnov,J.Curtis,and K.Narahari Rao,J.
          Mol.Spectrosc.79 (1980) 455

URB 81   S.Urban,V.Spirko,D.Papousek,J.Kauppinen,S.P.Belov,L.I.Gershtein,and
          A.F.Krupnov,J.Mol.Spectrosc.88 (1981) 274

WAY 76   F.D.Wayne,and H.E.Radford,Mol.Phys.32 (1976) 1407

WIN 71   G.Winnewisser,A.G.Maki,and D.R.Johnson,J.Mol.Spectrosc.39 (1971)
          149

WIN 79   M.Winnewisser,private communication (1979)

WON 82   M.Wong,I.Ozier,and W.L.Meerts,manuscript in preparation (1982)

WOS 75   P.Woskoboinikow,and W.C.Jennings,Appl.Phys.Lett.27 (1975) 658

WRI 78   G.T.Wrixon,and W.M.Kelly, 'Proc.3rd international conference on
          submillimeter waves and their applications',Guildford,U.K. (1978);
          Infrared Phys.18 (1978) 413

ZUI 77   B.F.J.Zuidberg,Ph.D.Thesis,Katholieke Universiteit Nijmegen (1977)

ZUI 78   B.F.J.Zuidberg,and A.Dymanus,Appl.Phys.16 (1978) 375

ZUI 79   B.F.J.Zuidberg,and A.Dymanus,Appl.Phys.19 (1979) 171

ZWE 68   S.Zwerdling,R.A.Smith,and J.P.Theriault,Infrared Phys.8 (1968) 271

Het experimenteel onderzoek dat in dit proefschrift staat be-
schreven, is gericht op hoge-resolutie spektroskopie in het
verre-infrarood met behulp van een monochromatische bron die
straling levert met kontinu verstembare frekwentie. Een deel
van het onderzoek is gewijd aan de ontwikkeling en verbetering
van de spektrometer, het andere deel aan de produktie en
spektroskopie van molekulen, radikalen en ionen.

Het eerste hoofdstuk is geschreven ter oriëntatie. Het
verre-infrarood is een gebied in het elektromagnetisch spek-
trum, dat (nog steeds) moeilijk toegankelijk is voor hoge-
resolutie spektroskopie, wegens het vrijwel ontbreken van
stralingsbronnen die direkt voor dit type onderzoek geschikt
zijn. In Hoofdstuk 1 wordt een globaal beeld geschetst van de
tot op heden gevonden oplossingen voor dit probleem. De unieke
spektrometer die voor het huidige onderzoek is gebruikt werd
in eerste versie reeds ontwikkeld, voordat het hier beschreven
onderzoek werd gestart. Het basis-idee om een frekwentie-
verstembare bron te maken door menging van een laser en een
mikrogolfbron met behulp van een diode wordt opnieuw belicht.

In Hoofdstuk 2 zijn de meest essentiële delen van de spek-
trometer beschreven. Extra aandacht is daarbij besteed aan
kwasi-optische technieken, geintroduceerd in het verre-infra-
rood ter verhoging van de efficiëntie van het mengproces.

Alle voor het merendeel spektroskopische resultaten zijn
samengevat in Hoofdstuk 3. Spektra zijn gemeten van enkele
molekulen, radikalen en ionen rond een frekwentie van 1 THz,
met een oplossend vermogen van ongeveer 3 MHz. In het geval van
radikalen is speciaal de fijn- en hyperfijn struktuur in
rotatiespektra bestudeerd. Dit heeft geleid tot de bepaling (of
verbetering) van molekulaire konstanten die maatgevend zijn voor
de sterkte van diverse interakties binnen deze radikalen. De
spektroskopie van vrije ionen in de gas-fase heeft de laatste
jaren een toenemende belangstelling genoten. Van deze deeltjes
is spektroskopisch nog relatief weinig bekend, doordat vrije
ionen in het laboratorium moeilijk in voldoende grote koncen-

traties (ca. 10^{10} cm^{-3}) te produceren zijn. Het is niettemin gelukt met de huidige spektrometer enige ionen te bestuderen. De eerste resultaten van het ionenexperiment, dat in het derde hoofdstuk is beschreven, tonen op zijn minst aan dat de spektrometer zeer geschikt is voor verder onderzoek in deze richting. Verder is aangetoond dat het mengproces met de diode ook bij zeer hoge frekwenties (2.6 THz) efficiënt plaats vindt. Dit betekent dat de gebruikte techniek voor het genereren van straling met verstembare frekwentie, toepasbaar is in het volledige verre-infrarood tot een frekwentie van ongeveer 4 THz.

Het proefschrift wordt afgesloten met enige bespiegelingen over toekomstig spektroskopisch onderzoek.

CURRICULUM VITAE

Op 25 december 1953 ben ik geboren te Velp (G). De middel-
bare schoolopleiding volgde ik aan het Thomas a Kempis
College te Arnhem en behaalde in 1970 het diploma HBS-B.
Aansluitend werd de studie wis- en natuurkunde begonnen
aan de Katholieke Universiteit Nijmegen. Het kandidaats-
examen werd behaald in 1974, het doktoraalexamen experimen-
tele natuurkunde in november 1977. Tijdens mijn afstudeer-
periode verrichtte ik experimenteel werk binnen de werkgroep
Atoom- en Molekuulfysika. Na het doktoraalexamen kreeg ik
de gelegenheid binnen dezelfde werkgroep een promotie-
onderzoek te verrichten. Onder leiding van Prof.Dr.A.Dymanus
leverde dit onderzoek de resultaten op die in dit proefschrift
zijn beschreven.